Radiation Physics and Chemistry 204 (2023) 110715

Contents lists available at ScienceDirect

Radiation Physics and Chemistry

journal homepage: www.elsevier.com/locate/radphyschem

Physical and digital phantoms for 2D and 3D x-ray breast imaging: Review on the state-of-the-art and future prospects

Antonio Sarno [a,*], Chiara Valero [b], Raffaele M. Tucciariello [c], Nikolay Dukov [d], Paulo R. Costa [e], Alessandra Tomal [f]

[a] Università di Napoli "Federico II" Department of Physics "E Pancini" and INFN sez di Napoli, Napoli, Italy
[b] Azienda Ospedaliera Ordine Mauriziano, Medical Physics Department, Torino, Italy
[c] Centro di Riferimento Oncologico della Basilicata (IRCCS-CROB), Fisica Sanitaria, Rionero in Vulture, Potenza, Italy
[d] Medical University of Varna Department of Medical Equipment, Electronic and Information Technologies in Healthcare, Varna, Bulgaria
[e] Instituto de Física/Universidade de São Paulo, São Paulo, Brazil
[f] Instituto de Física Gleb Wataghin, Universidade Estadual de Campinas, Campinas, São Paulo, Brazil

ARTICLE INFO

Keywords:
Breast phantoms
Mammography
DBT
BCT
Additive manufacturing
Virtual clinical trials

ABSTRACT

Breast phantoms are a fundamental asset both in routine quality assurance programs and for comparing scanner performance in 2D and 3D x-ray breast imaging. They also play an essential role in the optimization of imaging systems and for testing new technologies before their introduction in the clinical practice. The ideal phantom must reflect and mimic the organ anatomy and pathologies, including details such as simulated tumor masses or microcalcifications. They can also be designed to evaluate a particular technical specification of the detector or of the imaging setup, such as noise or spatial resolution.

The introduction of digital breast tomosynthesis (DBT) and computed tomography dedicated to the breast (BCT) in the clinical practice allowed to acquire 3D breast images with relatively high contrast and spatial resolution. The introduction of these innovative technologies encouraged the development of new phantoms for quality assurance and systems comparisons; on the other hand, 3D images of the breasts acquired with DBT and BCT apparatuses along with innovative and low-cost additive manufacturing technologies have been the basis for the development of a new class of digital and physical anthropomorphic breast phantoms. In these cases, the realism has been demonstrated to be fundamental in overtaking the limits of conventional phantoms used in digital mammography (DM) quality assurance programs.

This work aims at reviewing the conventional phantoms adopted for testing and optimizing DM, DBT and BCT systems and to furnish a critical insight in emerging physical and digital breast phantoms. The limitations of conventional phantoms will be outlined, also regarding the needs of comparing apparatuses which adopt a compressed breast geometry to modern BCT ones, with pendant uncompressed breast geometry.

1. Introduction

The introduction in the clinical practice of the digital breast tomosynthesis – DBT – (Niklason et al., 1997; Sechopoulos, 2013a; 2013b) and of the dedicated breast CT – BCT – (Sarno et al., 2015) for breast cancer detection and diagnosis requires new classes of breast phantoms for the systems testing, evaluations and developments. These brand-new phantoms must serve in the evaluations of the imaging performance and dose levels of the scanners, for the design and the optimization of the apparatuses and as a support in the regulatory submissions, replacing the randomized clinical trials on patient populations (Glick and Ikejimba, 2018). In DBT, multiple acquired projections of the compressed breast over a limited angular range allow the reconstruction of pseudo-3D image volumes as slices parallel to the detector plane. This reduces the tissue overlapping of the projection images characterizing conventional 2D mammography – DM – that may hinder the cancer diagnosis. However, moving from 2D to pseudo-3D DBT imaging may compromise the use of some phantoms routinely adopted in 2D apparatus testing. Hence, these are devised for 2D technologies and are not meant to take into account for the impact of the reduction of tissue superimposition in a structured background (Strudley et al., 2015; Vancoillie et al., 2021). Although conventional phantoms - composed by

* Corresponding author.
E-mail address: sarno@na.infn.it (A. Sarno).

https://doi.org/10.1016/j.radphyschem.2022.110715
Received 5 July 2022; Received in revised form 22 November 2022; Accepted 7 December 2022
Available online 9 December 2022

homogeneous material background and embodying details for image quality testing - are still recommended for quality assurance (QA) tests in DBT (EUREF, 2018; ACR, 2018), they may not be adequate for comparing 2D and 3D imaging systems and they can also be not adequate for comparisons between different 3D systems, where the third dimension of the reconstructed images may be considered the most important addendum of the technology. In BCT, 3D breast volume is reconstructed from projections acquired over 360° scan angle. In this modality, the imaged breast freely hangs from a hole on the support, which bears the patient in prone position and the firm organ compression of DM and DBT is not applied. As a result of the fully 3D imaging technique, the anatomical noise due to the breast tissue parenchyma is further reduced in BCT (Chen et al., 2013). This uncompressed geometry requires phantoms capable of evaluating the advantageous reduction of the anatomical noise and its impact on lesion detectability also in comparison to DM and DBT. In addition, the use of the tomographic technique and reconstruction algorithms in both DBT and BCT can be sources of artifacts absent in 2D DM (Geiser et al., 2018), which need to be evaluated with appropriate phantoms in quality assurance protocols (Strudley et al., 2015; EUREF2018).

Along with the needs of devising new classes of phantoms, the 3D images of the breasts acquired with DBT and BCT apparatuses permitted an insight in the in-vivo anatomical structure of the organ and a refinement of the breast models (Boone et al., 2017). Hence, 3D images acquired with dedicated CT scanners can reach spatial resolution of few hundreds of micrometers, permitting to delineate and outline fine breast details and 3D tissue distribution (Huang et al., 2008, 2011; Sarno et al., 2015, 2016a; Gazi et al., 2015; Kuttig et al., 2015; Longo., 2019; Caballo et al., 2018a). This has already shown its impact in x-ray breast imaging dosimetry where the conventional assumption of the skin tissue (Huang et al., 2008; Sarno et al., 2016b, 2019, 2021a; Massera and Tomal, 2018) and homogenous glandular tissue distribution (Sechopoulos et al., 2012; Hernandez et al., 2015; Sarno et al., 2018a, 2018b, 2022) have been confuted towards a redefinition of the dosimetric paradigms in the x-ray breast imaging (AAPM TG282).

The availability of sophisticated digital breast phantoms is a fundamental asset in the development of platform for virtual clinical trials (VCT) (Bakic et al., 2002a, 2002b, 2003, 2018; Badal et al., 2018, 2021; Sharma et al., 2019; di Franco et al., 2019; Sarno et al., 2020; Barufaldi et al., 2021, 2022; Mettivier et al., 2022a; Marshall and Bosmans, 2022). VCT are in-silico reproductions of clinical trials on patient populations with a computed model of the imaging chain and digital patients replacing the human ones. In this context, the digital breast phantom must reproduce as fair as possible the breast anatomy and silhouette or, similarly, must permit the computation of images with realistic features. The advantages of this innovative approach for medical device evaluations reside in the reduction of time, costs and patient risks, also toward an acceleration of processes for approval and regulatory (Badano, 2021). In addition to be an irreplaceable part of VCT platforms, sophisticated digital breast phantoms may also play an important role in manufacturing innovative physical breast phantoms. In particular, with the advent of additive technologies in the medical physics field, digital breast models may furnish the appropriate design for devising physical breast phantom with anthropomorphic features (Bliznakova, 2020).

In the background of the refinement of breast models offered by innovative imaging technologies and the introduction of additive manufacturing for devising new classes of breast phantoms with realistic features, this work aims to review the state-of-the-art and furnishing a horizon scanning of emerging physical and digital phantoms adopted for investigations in 2D and 3D x-ray breast imaging. The first part of the review will be dedicated to the description of the currently adopted phantoms, with particular focus on those proposed in worldwide QA protocols. Emerging phantoms and state-of-the-art phantoms will be described in the light of new challenges due to the introduction of DBT and BCT in the clinical practice and the needs related to the comparison of these new imaging technologies to the conventional 2D DM. New phantoms design and materials will be described, with these aiming both at introducing anatomical complexity to the conventional homogeneous phantoms and at extending the usability of employed materials to broader photon energy ranges, which can reach up to 80 keV in BCT (Sarno et al., 2015). In particular, this review will describe the advancement in 3D printed breast phantoms, a promising class of phantoms featuring the virtue of the great possibility of customization. Proposed breast models and phantoms will be presented in the light of criticisms related to the limitations of the different proposals and looking at potentials they can offer both in VCT and in new challenges related to the evaluation of image quality of 3D x-ray breast imaging apparatuses. With the selection of the appropriate materials for breast phantom being a fundamental aspect in the manufacturing chain, the final part of the review will furnish an overview on the used evaluations approaches proposed in the field.

2. Conventional breast phantoms

2.1. Dose assessment in international QA protocols

In order to evaluate the Average Glandular Dose (AGD) (Dance and Sechopoulos, 2016) in routine QA tests in DM and DBT, polymethyl methacrylate (PMMA) slabs are commonly adopted as breast phantom (IPEM, 2005; EUREF, 2006, 2018; NHS, 2009, 2015; IAEA, 2011; EFOMP, 2015). The PMMA blocks are firstly exposed in AEC mode in order to verify system technique factors (tube voltage, mAs and anode/filter combination) selected by the unit for the equivalent compressed breasts, then, on the basis of such parameters, the AGD is estimated on the basis of the measurements of incident air kerma on the breast surface. Since PMMA is denser than breast tissues, different PMMA thicknesses have been scaled to identify certain equivalent compressed breast thicknesses (Dance et al., 2000). As example, Table 1 shows equivalence between PMMA thickness and breasts as adopted in the EUREF (2006) protocol along with limiting AGD levels.

The new EUREF (2018) QA protocol has extended the use of PMMA slabs to the case of DBT, uphold the PMMA as a proper test object and provided the same procedure followed for 2D mammography for AGD estimates based on Dance et al. (2010). The same methodology is shared by international and national agencies and services, such as IAEA (2011) and NHS (2015).

Although the use of a universal test object simplifies the dose assessment procedure, it presents some limitations with the automatic selection of tube voltage, target or filter, based on the object thickness that may be slightly different from that for real compressed breasts. Hence, limits due to the use of PMMA slabs phantoms can be ascribed to its constant thickness and homogeneous composition which may prevent the replication of the AEC system operation of the case of exposition of heterogeneous breasts (Fedon et al., 2019). First, the phantom thickness could be corrected by adding layers of low absorbing materials to the PMMA (e.g. polyethylene - PE) to match the desired equivalent breast thickness, or by using spacers which create an air gap between the

Table 1
PMMA thickness and thickness and glandularity of the equivalent breast as reported in EUREF (2006) along with limiting AGD values.

Thickness of PMMA (mm)	Thickness of equivalent breast (mm)	Glandularity of the equivalent breast (%)	Maximum AGD to the equivalent breast (mGy)	
			Acceptable level	Achievable level
20	21	97	<1.0	<0.6
30	32	67	<1.5	<1.0
40	45	41	<2.0	<1.6
45	53	29	<2.5	<2.0
50	60	20	<3.0	<2.4
60	75	9	<4.5	<3.6
70	90	4	<6.5	<5.1

PMMA block and the upper compression paddle (EUREF, 2018). A comparison between both methods has been published by Bouwman et al. (2015) who also suggest the use of PMMA+PE test object instead of the alone PMMA, since spacers might affect the sensor of AEC and consequently conduct to erroneous AGD estimations. In their comparison, Bouwman et al. (2015) concluded that "*phantom AGD values may not always be representative of mean AGDs within a population… This is because of differences in the AEC response to the distributions of (simulated) breast tissue in phantoms and real breasts.*"

The American College of Radiology (ACR) proposes the use of a breast phantoms accredited in accordance with the FDA Mammography Quality Standards Act (MQSA) and to be adopted both for AGD estimates and for image quality evaluations. The ACR phantom has been designed with the intent of covering most of the detector area and it is composed by a PMMA border and a wax insert containing simulated masses, microcalcifications and fibers. It is meant to mimic a 50% glandular breast with a compressed thickness of 42 mm and its use for AGD estimates is similar to that described for PMMA block, since it is used to select the technique factors for incident air kerma measurements.

2.2. Image quality evaluation in international QA protocols

Image quality evaluations represent a fundamental part of the QA process since imaging performance and optimization must be pursued during the x-ray machine clinical lifetime. Validated phantoms, instrumentations and methodologies should be used to represent the clinical tasks involved in x-ray breast imaging. Quantitative parameters should be verified during the time and the use of dedicated phantoms with inserts of low and high contrast supports these tasks.

PMMA breast phantoms with several thicknesses are also proposed for simple image quality evaluations, such as that of the image signal-to-noise ratio (SNR) and contrast-to-noise ratio (CNR). In this last case, an Al sheet is placed on the phantom as contrasting detail (EUREF, 2006; NHS, 2009). However, in order to determine the threshold contrast visibility, several protocols require to assess the visibility of circular discs with a diameter ranging between 0.1 mm and 2.0 mm, placed on a background with an attenuation thickness equivalent to 50 mm of PMMA (EUREF, 2006; NHS, 2009). This may be performed by employing the CDMAM phantom (EUREF, 2006), made of several PMMA slabs and an insert which contains gold discs with variable diameter and thickness (contrast). Via an observer study - performed by experienced observers or automatized analysis - the minimal contrast visibility is determined. Fig. 1 shows a mammogram of a CDMAM phantom and the related contrast-detailed curve computed via an automatic analysis software.

The TORMAM phantom (NHS, 2009, 2015; EUREF, 2018) is suggested as a possible alternative to CDMAM. Specific details such as fibers and calcifications are also embedded in an anatomically realistic background. A similar phantom, the TORMAX is also suggested by NHS (2009) as a valid substitute to the CDMAM. However, QA protocols tests employing either CDMAM or TORMAM phantoms are designed for DM and may present some limitation when used in DBT, also preserving "an important role in stability assessment and quantifying some aspects of image quality" (EUREF, 2018).

As already mentioned in the previous section, ACR (2018) proposes the use of the accredited ACR phantom also for image quality evaluation both in DM and DBT. The ACR (2018) protocol provides a scoring method that exploits the embedded details in order to quantify the visibility of the simulated lesions. In addition, inclusions are used for the evaluation of image SRN and CNR as well as the image spatial resolution, distortions and artifacts.

As regard to the BCT, there is still no availability of any internationally recognized QA protocol, and it is worth to quote the phantom proposed in the user's manual[1] of the Koning BCT scanner produced by Koning Health (www.koninghealth.com, GE – USA). The Koning BCT received the CE mark in 2012 and FDA approval for use in diagnostic examinations in conjunction with 2-view mammography in 2017. The proposed phantom mimics the pendulant breast as an acrylic cylindrical container with diameter of 13 cm and height of 10 cm. It contains water and two cylindrical inserts. One insert is made of BR12 materials (White et al., 1977) simulating the attenuation coefficient of the 50% glandular tissue and embodies 6 clusters of microcalcifications whose diameters range between 165 μm and 375 μm. The second insert contains a BR12 region with spherical masses whose reconstructed voxel values are supposed to differ by the BR12 background of about 30 HU. The diameter of the masses ranges between 2.5 mm and 10.5 mm and their presence aims at evaluating the low-contrast visibility of insertions. Outside the BR12 region, there are four cylindrical details with diameter of 12 mm made of different materials for the evaluation of the CT-number linearity (adipose, breast, muscle, and 200 mg/cc hydroxyapatite H). In addition, a tungsten wire with diameter of 50 μm is present for the evaluation of the system modulation transfer function (MTF).

2.3. Comprehensive breast phantoms for evaluation of image quality and lesion detectability

Although it is not specifically requested in QA international protocols, medical physicists commonly use comprehensive breast phantoms in routine evaluations (Tomal and Costa, 2017). These are selected for specific needs and aspects that may result in a specific context not considered in routine protocols, as well as for economic reasons or based on the phantom availability. Most of the available commercial phantoms include simulated lesions such as microcalcification clusters, spherical masses or fibers. In addition, they can also contain inclusions for the evaluation of the system's spatial resolution (i.e. edge, bar pattern, etc) or contrast. The Gammex DBT breast phantom (Gammex Inc., WI, USA) is an example. It is a layered composite phantom and each of the constituting layers is meant for specific assessments, such as the evaluation of the MTF, the CNR, artifacts, geometrical distortions or a graduate scale for verifying the chest-wall x-ray field coverage.

A second example is the CIRS (CIRS Inc., VA, USA) phantom model 011A (Fig. 2). It has an anthropomorphic shape and the background material presents the attenuation characteristics of 50% glandular breast tissue. The inclusions embedded in the CIRS mod. 011A phantom comprise simulated masses and calcification clusters, nylon fibers, a low contrast step-wedge and 2 bar patterns. Similarly, the breast equivalent CIRS 014A layered phantom (Sarno et al., 2016a) permits the evaluation of image quality and lesion visibility for different breast thicknesses in DM or the CIRS 022 breast phantom which embodies details simulating different contrast medium concentrations for image quality evaluation in contrast enhancement digital mammography (Klausz et al., 2018).

The customized phantom used at the Radboud UMC (Brombal et al., 2019) for mimicking the pendulant breasts in a BCT scanner geometry was produced by CIRS Inc (Fig. 3). The modular layer phantom presented a semi-ellipsoidal truncated shape with maximum diameter at the chest-wall of 164 cm and it is made of a 100% adipose equivalent material. It embodies spheres of epoxy resin simulating low contrast masses, $CaCO_3$ microcalcifications clusters and fibers with different sizes. In addition, it contains a slab that can allocate circular chips made of different materials.

It is also worth to mention the Quart mam/digi EPQC DM and DBT phantom (de las Heras et al., 2013) which has the unique feature of embedding the Landolt Ring Structures proposed as substitute of the

[1] https://www.accessdata.fda.gov/cdrh_docs/pdf13/P130025c.pdf, accessed on 06/01/2022.

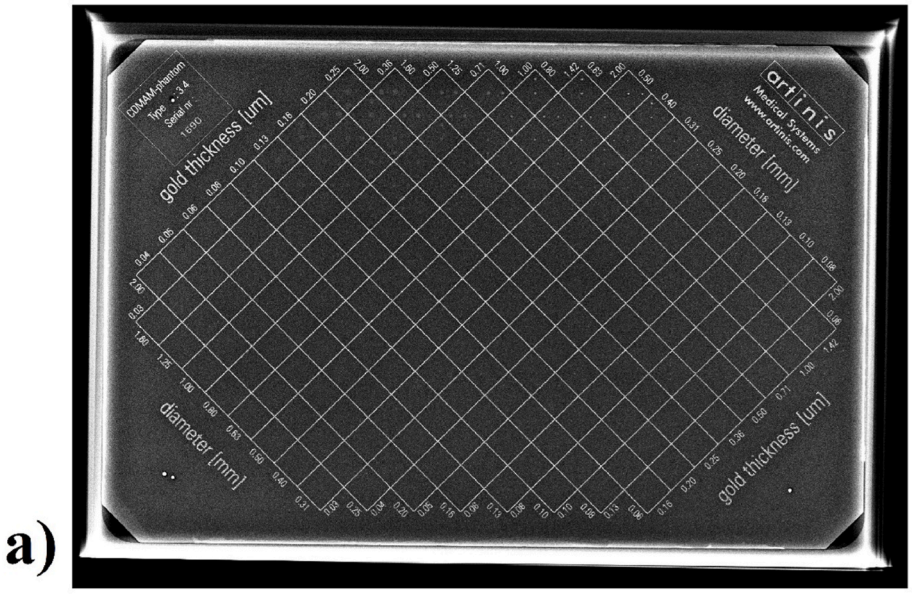

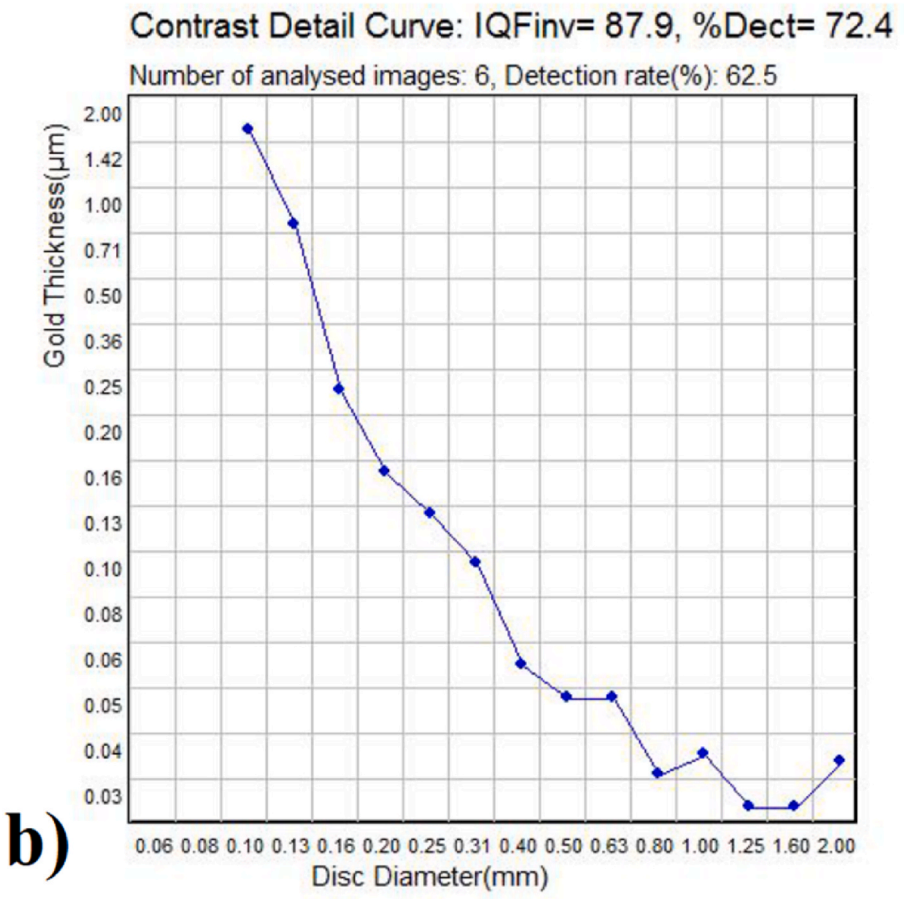

Fig. 1. a) Mammogram of CDMAM phantom Artinis type 3.4 acquired via a Hologic Selenia Dimension apparatus at 28 kV and b) the computed contrast-detail curve (Karssemeijer and Thijssen, 1996)

gold discs of the CDMAM phantom (de las Heras et al., 2013). The Quart phantom is proposed both for DM and DBT apparatuses QA tests and it is constituted by three semicircular PMMA slabs embodying different test objects such as contrast step wedges, MTF test object, low contrast stripes, references for missing tissue estimates and slots for dosimeters.

Although all these phantoms allow the evaluation of image quality and dose levels of the x-ray breast imaging systems - in particular with respect to reference values - and to comply with QA worldwide protocols, they all lack in reproducing the real breast parenchyma. This limits their use for absolute evaluation of the scanner capabilities, in particular where DBT and BCT systems are involved. Hence, the main advantage of these technologies resides in the reduction of the tissue

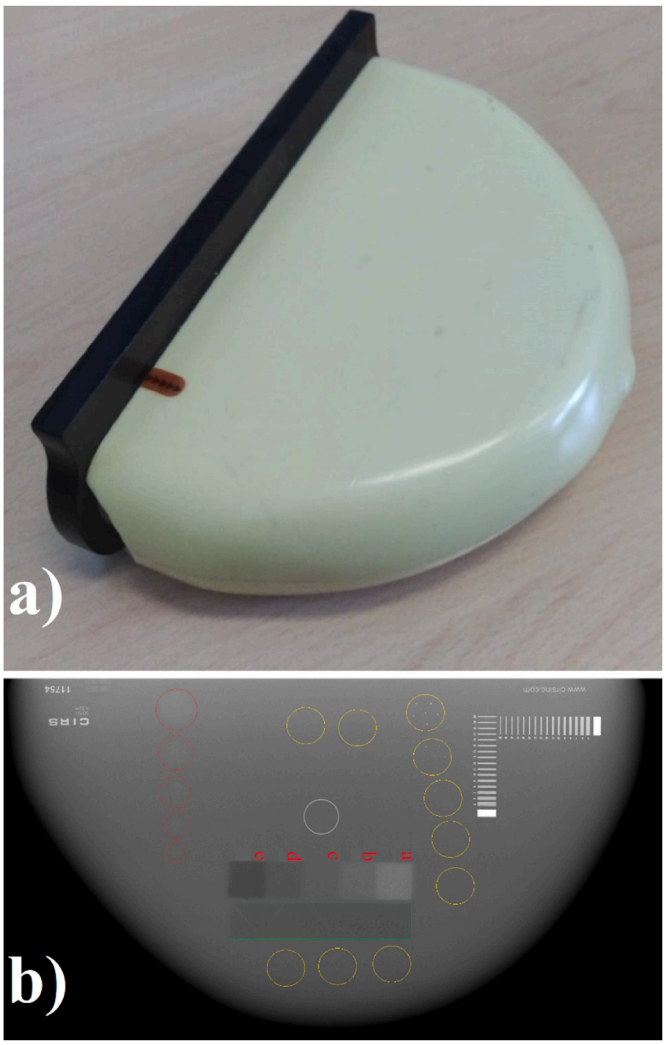

Fig. 2. Photo of the CIRS mod. 011A breast phantom and a slice from the reconstructed DBT images (Fujifilm DBT scanner, 24.8 mAs, 29 kV). It is constituted of a material mimicking the 50% glandular breast tissue and comprises several types of details: red circles outline visible hemispheric masses whose attenuation coefficient reflects those of 75% glandular breast; yellow circles outline visible microcalcification clusters; step wedge a-e is constituted of various 10 mm thick chips simulating attenuation coefficients of breast tissues whose glandular content goes from 100% (a) to 0% (e). Green rectangle outlines various nylon fibers and bar patterns are visible in the high-right corner of the slice (www.cirsinc.com).

overlapping present in conventional DM with a hypothetical enhancement of lesions detectability, hidden by anatomical noise in 2D projective mammograms. As already done for the TORMAM phantom (sect. 2.1), BR3D CIRS phantom model 020 and, optionally, DBT QA CIRS phantom mod 021 includes heterogeneous slabs meant to reproduce the 3D structure of the breast parenchyma (Glick and Ikejimba, 2018; Bliznakova, 2020) as a heterogeneous mixture of glandular-like and adipose-like materials. The β value - i.e. the absolute value of the slope of the image noise power spectrum (NPS) in log-log scale in an appropriate frequency range as quantification of the anatomical noise, Chen et al. (2012) - in mammograms and DBT slices of BR3D CIRS phantom (Cockmartin et al., 2013), resulted in line with the expected value of 3 assessed for the case of clinical images (Chen et al., 2012). This value was also reflected in the slope of the NPS of BR3D CIRS phantom images in Ikejimba et al. (2014). However, these phantoms do not reproduce the silhouetted of the real breast nor the 3D tissue variation over the organs.

A further issue in the use of conventional phantoms is related to the comparison of image quality in compressed geometry - proper of DM and DBT - to BCT, where the breast does not experience any compression. In this context, a phantom that may be adapted to the configuration under exam may be useful. In order to overtake this problem, Vollmar et al. (2009) proposed to use a cubic insert to be allocated either in the uncompressed pendant breast phantoms modeled as a 10 cm diameter and 10 cm height cylinder or in a phantom whose shape depicts that of 4.5 cm thick compressed breast undergoing DM or DBT. Both phantoms were made of BR12 material and adipose equivalent extensions were projected in case of need of larger models. The insert, supposed as a 4 cm × 4 cm × 4 cm cube, contained the necessary details for image quality evaluations, such as simulated tumors, fibers or calcifications, and it is opportunely allocated in the breast-shaped phantoms.

3. 3D breast imaging: new evidence for phantom innovations

3.1. Anthropomorphic digital breast phantoms

Anthropomorphic breast phantoms are physical (real) or digital (computational) and represent key tools for the evaluation of many aspects of the scanners, being useful for optimization or assessment of imaging systems, clinical commissioning or preclinical trials (Pokrajac et al., 2012; Abbey et al., 2019; Bliznakova, 2020). These phantoms provide a more realistic representation of complex breast anatomy in terms of its outer shape, the inner distribution of different tissues and the mammary parenchymal, modelling of pathologies and also simulate the physical properties of breast tissues (Bliznakova, 2020). The detailed representation of anatomical structures makes the anthropomorphic breast phantoms particularly useful for several tasks (e.g. detectability of lesions, image processing and reconstructions) (Bakic et al., 2002a, 2003; Bliznakova, 2020), being advantageous compared to the conventional phantoms with homogeneous background (Lau et al., 2012; Mettivier et al., 2017).

Recently, several computed models for generating anthropomorphic digital (*in-silico*) breast phantoms were developed and they have shown to be a practical alternative for testing new breast imaging modalities (Bliznakova, 2020). The possibility of knowing the ground truth and to explore a large variation of anatomical parameters of such breast phantoms offers innumerous advantages for quantitative evaluations, preclinical testing and optimization of parameters. The emerging VCT, which is an economical and flexible tool for evaluating diagnostic tasks in breast imaging systems, have been promoted by the evolution of digital breast phantom modeling and 3D breast imaging techniques, coupled with the simultaneous increase of computational power (Badano, 2021; di Franco et al., 2020; Elangovan et al., 2017; Mettivier et al., 2020; Sarno et al., 2021b; Sharma et al., 2019).

Anthropomorphic digital breast phantoms can be generated based on two approaches: i) generation from patient data and ii) generation relying on mathematical data (Bliznakova, 2020; Mahr et al., 2012). In the former approach (Fig. 4), a voxelized breast phantom is derived directly from clinical breast images, which are segmented with the purpose to identify the content of each voxel (Li et al., 2009; Erickson et al., 2016; Hsu et al., 2013; Elangovan et al., 2017; Garcia et al., 2020; Sarno et al., 2021b; Caballo et al., 2022). These patient-derived phantoms present the real silhouette and tissue distribution of the breast, although they are limited to the contrast, spatial resolution and voxel sizes of the classified images and to the segmentation methods. An additional limitation is the small cohort of available 3D images of the breast, mainly acquired via BCT scanners. In order to increase the number of the available cases, Sturgeon et al. (2017) proposed for example the use of a method based on Principal Component Analysis (PCA) for enlarging the patient-derived digital breast phantoms; the 600 generated virtual phantoms showed the same variability of the original dataset in terms of density and anatomical noise.

As regard to *in-silico* dosimetric studies, Fedon et al. (2018) showed that voxel sizes of the patient derived digital breast phantoms – usually

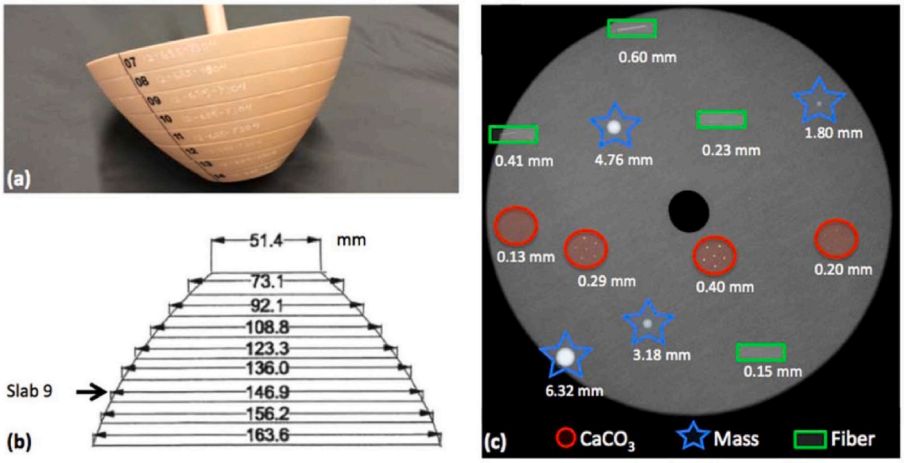

Fig. 3. a) Photo and b) a schematic of the BCT CIRS phantom at the Radboud UMC (The Netherlands). c) A coronal slice from the reconstructed CT image of the phantoms outlining the embedded inclusions. Reproduced from Brombal et al. (2019) under the Creative Commons Attribution 4.0 International License (http://creativecommons.org/licenses/by/4.0/).

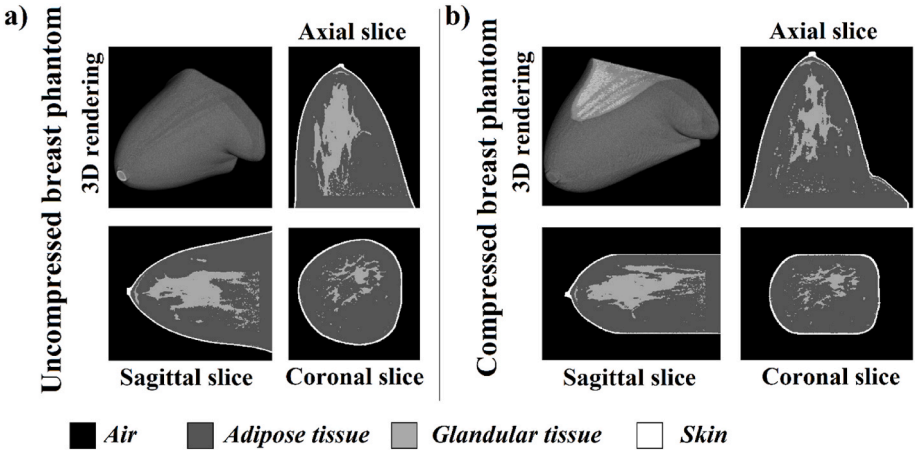

Fig. 4. Patient derived a) uncompressed and b) compressed digital breast phantoms from the dataset described in Sarno et al. (2018b) and available on zenodo.org (https://doi.org/10.5281/zenodo.4515360 and https://doi.org/10.5281/zenodo.4529852).

in the order of the voxel size of the original breast images whose edges range between 0.2 and 0.4 mm – is not a major issue. Hence, increasing the voxel sizes up to having an edge of few millimeters, resulted in having just a little influence on the computed dose via Monte Carlo simulations also with related benefits in terms of reduction of the computation time (Fedon et al., 2018). Patient-derived digital phantoms have been largely used for dosimetric assessments and studies (Sechopoulos et al., 2012; Hernandez et al., 2015; Sarno et al., 2017, 2018a, 2018b, 2022; Tucciariello et al., 2021), these outlining the limits of conventional homogeneous breast models and inspiring new paradigms for AGD calculations (Caballo et al., 2022).

The very high spatial resolution of DM and DBT systems - up to several times better than that of BCT scanners whose images are used for deriving 3D breast phantoms - may question the use of this patient-derived class of phantoms for *in-silico* reproduction of the imaging chain. The work of Caballo et al. (2018b) coped with this issue and relying on a supervised machine learning algorithm trained on high-resolution 3D breast images, made an attempt for reducing the voxel size of digital breast phantoms derived from a clinical BCT scanner.

Since the patient-derived digital breast phantoms are mainly derived from images of the uncompressed breast acquired with BCT scanners, the classified digital models need to be manipulated in order to reach the shape and silhouette of the compressed organ undergoing simulated DM or DBT. The software presented in Zyganitidis et al. (2007) – that is based on the knowledge of the elastic properties of the involved materials and the final compression thickness – was successful adopted in Sechopoulos et al. (2012) and in Sarno et al. (2021b) (an output example is shown in Fig. 4b) demonstrating that the modification of the glandular tissue percentage during the compression is contained. Similar results were obtained in Garcia et al. (2020), who adopted the open-source software NiftySim (v.2.3.1; University College London, UK) for computing the compression of the organ digital model.

On the other hand, digital breast phantoms derived from mathematical models simulate the elements of the breast based on anatomical assumptions, representing the external breast shape, mammary ducts, Cooper's ligaments, vessels, skin and breast lesions (Bakic et al., 2002a, 2003, 2011; Bliznakova, 2020; Bliznakova et al., 2003, 2010; Graff, 2016; Ikejimba et al., 2017a; Lau et al., 2012; Pokrajac et al., 2012; Zyganitidis et al., 2007). The mathematical modelling allows to produce an unlimited number of breast phantoms covering a wide spectrum of breast anatomical characteristics. Voxel size of breast models based on mathematical data are not limited as in the case of those derived from clinical images, but can be opportunely tuned.

One of the first 3D anthropomorphic digital breast phantom was developed by Bakic et al., 2002a, 2003 – UPenn digital breast model –

being based on a realistic distribution of large and medium anatomical structures. The large-scale structures were built based on two ellipsoidal regions, predominantly compose by adipose tissue or fibro-glandular tissues. The medium scale elements were modeled as adipose compartments and breast ductal network, which were mathematically modeled by realistically distributed elements: shells, blobs and the ductal tree. The pattern of ducts was modeled by a random binary tree model, representing probabilities of branching at different levels of a tree structure, being compared to ducts from galactogram images. The compressed breast model for 2D images was generated based on a breast deformation model and tissue elasticity parameters. A more realistic representation of adipose compartments and Cooper's ligament was achieved using a seeded region-growing algorithm (Bakic et al., 2011). The variations in breast anatomy (i.e., different size, glandularity, and adipose compartment distributions) were implemented through modification of the model. Further developments proposed a new algorithm for computer simulation of breast anatomy that allowed to generate high resolution anthropomorphic breast phantoms with voxel size in the range of 25–1000 μm^3 (Pokrajac et al., 2012), combining large- and small-scale features (Lau et al., 2012). The UPenn anthropomorphic breast phantoms - improved over the years - have been extensively used for simulation of 2D and 3D breast imaging techniques in VCT (Abbey et al., 2019; Bakic et al., 2018a; Barufaldi et al., 2018, 2020, 2021; Borges et al., 2019; Maidment et al., 2018; Vimieiro et al., 2019). Finally, this mathematical model was also used as basis for construction of physical anthropomorphic breast model (Carton et al., 2011, see following sect. 3.2.1).

Bliznakova et al. (2003) also described a 3D digital breast phantom for x-ray breast imaging simulations that allowed the generation of realistic 3D uncompressed breast models. Such models were based on complex aggregates of a breast external shape, ductal lobular system, Cooper's ligaments, pectoralis muscle, 3D mammographic background texture and breast abnormalities. The computer modelling of the breast adopted a combination of 3D geometrical primitives to represent the many parts of the breast anatomy: the breast shape was modeled by an elongated semi-ellipsoid and a semi-hyperboloid; network of cylinders, probabilistically arranged, simulates the duct system; cone-shaped object models the pectoralis muscle; ellipsoid shells at randomly sampled positions simulate the Cooper's ligament; spheres and ellipsoids to simulate regular shaped abnormalities; voxel matrices aim at simulating the 3D mammographic background texture or irregularly shaped abnormalities in computed images. Further studies improved the methodologies and permitted the development of the *BreastSimulator* software platform (Fig. 5) (Bliznakova et al., 2010, 2012), which allowed the inclusion of lymph nodes, blood vessels and the skin, all of them modeled by primitive geometrical and absent in the previous version (Bliznakova et al., 2003). This platform permitted the customization and the generation of the digital breast phantoms, allowing the user to input the multiplicity and dimensions of the primitives constituting the desired breast model (Bliznakova et al., 2010, 2012). An additional module of the *BreastSimulator* platform implemented the compression algorithm described in Zyganitidis et al. (2007) aiming at producing breast phantoms to be used for *in-silico* DM and DBT computations and a dedicated part of the software analytically computes x-ray breast projections. In addition, a new algorithm for 3D mammographic texture generation was modeled based on the concept of the fractional Brownian motion model, aiming to represent breast structures that are not explicitly modeled (Bliznakova et al., 2010). Finally, all geometrical primitives are transformed to voxel values of the final breast matrix. The resulting breast models permitted a fair reproduction of the parenchyma structure and anatomical noise in simulated breast images (Mettivier et al., 2017). The software application *BreastSimulator* have been extensively used to generate realistic breast models to evaluate new imaging techniques (Malliori et al., 2014; Mettivier et al., 2016) and also as computational prototypes for manufacturing anthropomorphic physical breast models (Feradov et al., 2019).

A new anthropomorphic digital breast phantom model was developed by Graff (2016) by generating random voxelized breast models with voxels of arbitrary sizes, aiming at representing the anatomic variability observed in women population. Such breast models include different tissues: skin, nipple, lactiferous duct, terminal duct lobular unit, inter-lobular glandular tissue, fat, Cooper's ligaments, chest muscle, arteries and veins. The shape of the breast surface is created from a base quadric, following a series of deformations and then a voxelized skin layer, a nipple and a pectoralis muscle are added. The initial glandular compartments in the interior of the surface are generated using a random Voronoi technique. The ductal tree structure is grown using a random branching algorithm from the nipple into each

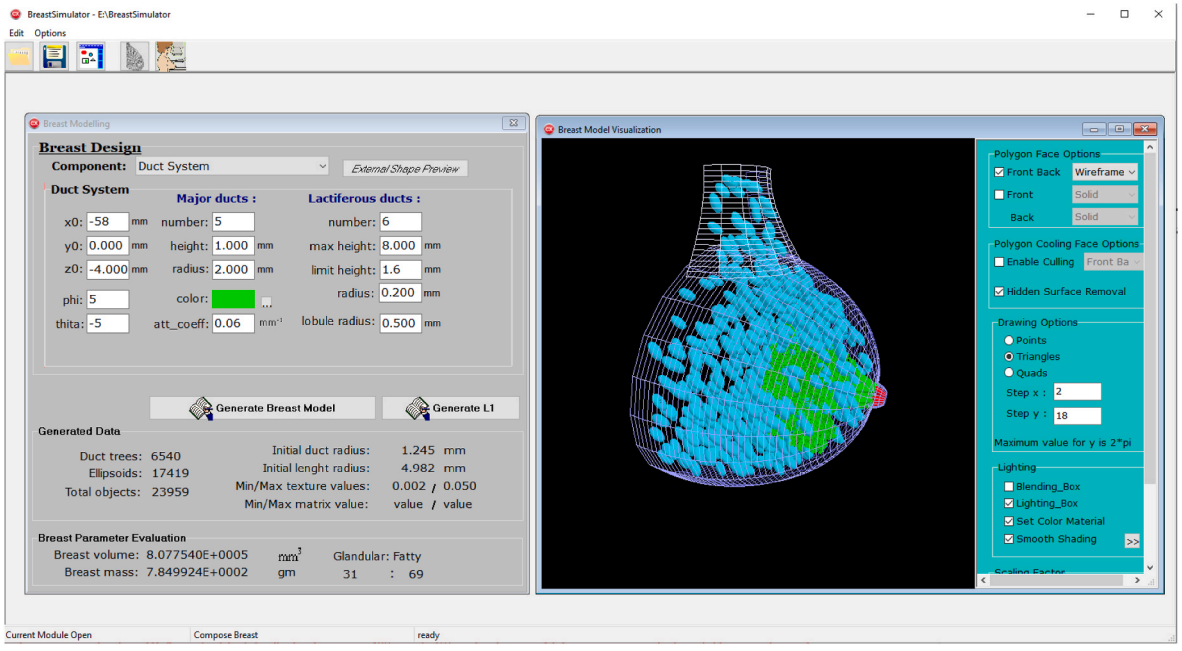

Fig. 5. Screenshot of the *BreastSimulator* software interface. It permits to input the desired model characteristics and to visualize the created digital breast phantoms. The picture was kindly provided by prof. K. Bliznakova from the Medical University of Varna (Bulgaria).

compartment. Random fat lobules are included within the inner regions, where the lobules number and size are adjusted to create phantoms with specific glandular content. The same approach is used to include the Cooper's ligaments. A vascular tree grown from the chest muscle is generated. Breast phantoms with different characteristics (volume, glandular content, duct radius, etc.) can be generated based on two approaches: randomly sampled from a population-based distribution or chosen by the user by selecting a specific set of model parameters. Compression of breast models is simulated by using a neo-Hookean elasticity model implemented via finite element techniques using the FeBio software package (www.febio.org). This digital breast phantom model has been extensively used for several applications in breast imaging and VCT (Badano et al., 2017, 2018; Sharma et al., 2019) and as input for producing physical breast models (Ikejimba et al., 2017a, 2017b, see following section).

The detailed breast model *DeBRa* focused on modelling both compressed and uncompressed breasts (Ma et al., 2009), creating a high-resolution, organ-specific hybrid phantom for general-purpose Monte Carlo studies. The mathematical breast model based on geometric structures mimicking the breast shape and the anatomic structures included several parts such the lactiferous duct system, the Cooper ligaments and the pectoral muscle. Mahr et al. (2012) built a framework for the construction of realistic 3D virtual breast phantoms based on a stochastic model derived entirely from mathematical equations based on statistical observations of the tissues of the breast. The outer breast boundary was defined by fitting geometrical functions, such as ellipsoid and series of second-degree polynomials. The specific structures of the breast subcutaneous fat layer and fibroglandular regions, subcutaneous–fibrous surface, intraglandular fat, Cooper's ligaments, lobules and duct structures were modeled by a random distribution of geometrical shapes.

Finally, anthropomorphic breast phantoms that include breast abnormalities have been of eminent interest for implementing VCT. In this context, several works have described the developing of mathematical models of clinical breast lesions (Bakic et al., 2018b; Bliznakova et al., 2019; Dukov et al., 2019a), while a database which summarizes the main examples of these models was published in the last years (Bliznakova et al., 2019).

3.2. Anthropomorphic physical breast phantoms

3.2.1. 3D printed breast phantoms

In recent years, additive manufacturing and 3D printing technology have been introduced as innovative approaches for devising phantoms for medical physics applications as well as for investigations in x-ray breast imaging (Bliznakova, 2020).

Main advantages are related to the production variable costs lower than prices of conventional phantoms as well as to the unique possibility of producing physical models of the organs starting from any arbitrary digital model. Such an arbitrariness allows to overtake the characteristics of conventional breast phantoms which present the main limitations in the homogeneous or quasi-homogeneous background (Varallo et al., 2022), and silhouette which largely differs to that of the real breasts. Main concerns related to the use of 3D printing technologies are the limited availability of the materials - these required to present the same physical characteristics (i.e. cross section for the energy range of interest of the x-ray system) of the breast tissues – and the scarce possibility of combining them in multi-material phantoms for reproducing the different tissues (Kiarashi et al., 2015; Ikejimba et al., 2016a; Sikaria et al., 2016; Zhao et al., 2017; Glick and Ikejimba, 2018; di Franco et al., 2019; Rossman et al., 2019; Schopphoven et al., 2019; Georgiev et al., 2020; Dukov et al., 2022; Varallo et al., 2022).

While 3D printing indicates general processes for manufacturing objects from digital files, there are several 3D printing technologies with different features that have been explored for phantom manufacturing in x-ray breast imaging field. Stereolithography (SLA) allows to manufacture phantoms by means of a UV light source, which selectively cures photopolymer resins; similarly, Selective Laser Sintering (SLS) permits to sinter powder materials. Both SLA and SLS were proposed for breast phantoms manufacturing (Bliznakova, 2016; Ivanov et al., 2018; Mainprize et al., 2018, 2020; Esposito et al., 2019; Bliznakova et al., 2020; Malliori et al., 2020). Main features of these two 3D printing techniques may be found in the capabilities of reproducing details with fine resolution in the manufactured objects in the order of tens of micrometers; however, the printing process accepts one material at time, compromising the possibility of devising breast phantoms that embody more than one substitute tissue. This disadvantage confines the use of the SLA and SLS processes to the production of simple phantoms mainly used as container (Bliznakova, 2016; Bliznakova et al., 2020) or simulated lesions and inclusions (Dukov et al., 2019b, 2020). The fine structure of the duct tree for example can be easily printed via SLA technology, as well as specific compartments of the phantoms such as adipose compartments (Dukov et al., 2020). Cockmartin et al. (2017) used SLA technology for the manufacturing of both spiculated and non-spiculated breast lesions from digital models derived from clinical images (Shaheen et al., 2014). The printed lesions were embodied in a customized phantom with a PMMA enveloped and filled with water and PMMA spheres meant to replicate the anatomical noise present in breast clinical images (Gang et al., 2010; Cockmartin et al., 2015).

In order to make SLS phantoms to mimic the real breast anatomy, including the complexity of the breast parenchyma, Mainprize et al. (2018, 2020) developed a phantom replicating the sole adipose compartments of the breast manufactured by curing polyamide-12 material, this found suitable as substitute for adipose tissue. Afterwards, in order to include also a substitute of fibro-glandular tissues, a low-viscosity resin was poured in order to fill-up the empty spaces and oven cured. Several vacuum cycles at 0.1 kPa permitted to reduce the air trapped in the phantom and the inclusion in the resin of zinc-oxide nanoparticles permitted to tune the attenuation properties of the materials. Measurements of the attenuation coefficients of samples of the 3D printed polyamide-12 and of the cured zinc-oxide doped resin were used to validate them as substitute of the adipose and glandular breast tissues, respectively (Mainprize et al., 2020). Images of the phantom on clinical DM/DBT apparatuses showed that this approach permitted to obtain images close to those simulated via the 3D digital breast model at the basis of the manufacturing process (Mainprize et al., 2020). A similar process was also followed by Malliori et al. (2020), who used SLA 3D printing technique for manufacturing molds mimicking the skin envelope and the fibroglandular parenchyma; afterwards the empty spaces were filled with paraffin to simulate the adipose background. The absence of the vacuum process in this case made air bubbles visible in tomographic images of the breast phantoms, these come up from the paraffin infilling processes.

Fused deposition modelling 3D printing technology (FDM, also known as fused filament fabrication – FFF) allows the manufacturing of 3D phantoms starting from thermoplastic materials that are melted while passing through a heated extruder nozzle and are deposited layer-by-layer on a heated platform. In comparison to SLA and SLS technologies, FDM creates objects with lower definition in the order of hundreds of micrometers. This may determine the presence of patterns related to the printing processes stratification which are visible in the high-resolution images of the phantom acquired with mammographic scanners (Clark et al., 2016; Varallo et al., 2022). These defects may be mitigated using suitable printing patterns (Dukov et al., 2022). The use of single-extruder FDM printers presents the same limitation of the SLS and SLA technologies related to the manufacturing of phantoms containing more than one material. Hence, this technology has been proposed for the manufacturing of single inclusions, for the organ container/skin or for phantoms assembled from multiple pieces (He et al., 2019; Dukov et al., 2019b; Maillori et., al 2020; Germann et al., 2021). Fig. 6 shows a breast phantom developed at the Medical University of Varna (Dukov et al., 2019b) whose skin envelope and tumor

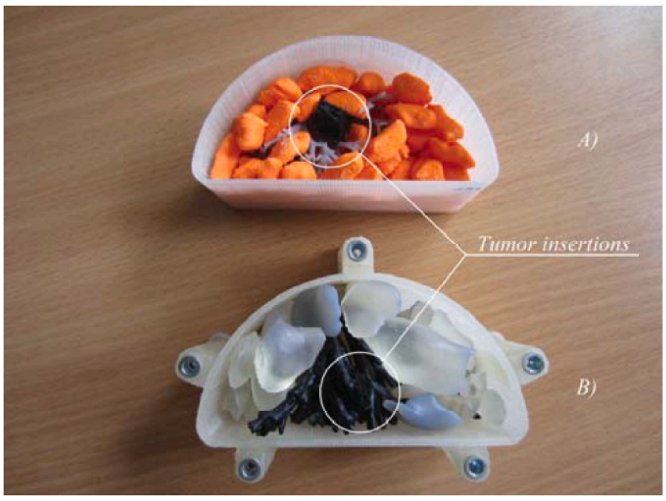

Fig. 6. Modular breast phantoms 3D printed at the Medical University of Varna (Bulgaria). The envelopes and the simulated tumors are manufactured with FDM technology and adipose compartments are developed via SLA technology. The duct tree is developed by means of FDM in a) and SLA in b). © 2019 IEEE. Reprinted, with permission, from Dukov et al. (2019b) An approach for printing tissue-mimicking abnormalities dedicated to applications in breast imaging. In 2019 IEEE XXVIII International Scientific Conference Electronics (ET) (pp. 1–4), IEEE.

have been developed by means of FDM technology; the complete phantom assembly comprises also adipose compartments made of epoxy resins and 3D printed via SLA technology as well as duct trees, manufactured via SLA technology in Fig. 6a and via FDM printer in Fig. 6b.

Malliori et al. (2020) have also replicated their approach for the production of multi-material breast phantoms by employing SLA technique to the FDM case. They produced breast molds made of ABS, Hybrid, Nylon, PET-G and PLS for mimicking the breast envelope and the fibroglandular parenchyma. The printing settings included 100% infill factor, 0.1 mm layer resolution and linear pattern; also in this case the inner portion of the mold was filled with paraffin for simulating the adipose compartments. However, in the case of FDM phantoms, in spite of the use of 100% infill factor, printing patterns and hollow areas are evident in the 2D projection images of the phantoms, making this technique less suitable than SLA, where no patterns were evident.

The use of FDM 3D printers equipped with more than one extruder permits to create breast phantoms made of more than one material reproducing patient derived and anatomical realistic digital breast models (di Franco et al., 2019; Varallo et al., 2022). With the attenuation coefficients of the breast tissues being characterized in three mainly components usually identified as representing the skin, adipose and glandular tissues (Caballo et al., 2018a; Sarno et al., 2021b), it would be necessary printing at least three different materials at time. It may be obtained by devising the inner portion of the organ comprising the adipose and the glandular compartments as a single embedded block and a removable external envelope as skin substitute (di Franco et al., 2019; Varallo et al., 2022). As alternative, it can be considered that the skin layer is an outer thin layer of 1.45 mm on average (Huang et al., 2008; Shi et al., 2013) and may have scarce influence on the phantom images or that its attenuation is close to that of the glandular tissue (Ivanov et al., 2018). On the bases of this assumption, the use of a two-extruder FDM printer will be sufficient for the production of embedded breast phantoms with both glandular tissue and skin reproduced with the same material (Varallo et al., 2022). This permits to have the skin layer attached at the inner bulk reducing the interface gape due to the separate layers (Varallo et al., 2022). Fig. 7 reports a picture of the breast phantoms produced with a two-extruder FDM printer at the University of Naples (Italy) whose skin and glandular regions were reproduced with the same material. These phantoms were manufactured starting from digital breast phantoms derived from clinical breast images acquired via dedicated BCT scanner; as first step (see also sect. 3.1), clinical images of the uncompressed breast were segmented and each voxel classified as containing adipose tissue, glandular tissue or skin (Sarno et al., 2021b). The output from this classification process constituted the design at the basis of the manufacturing of uncompressed physical breast phantoms for BCT testing and evaluations (di Franco et al., 2019). A computed compression allowed to generate digital breast phantoms for the same "digital patient" constituting the design of the compressed version of the 3D printed physical breast phantom (Varallo et al., 2022). The main advantage of this approach is represented by the possibility of having both compressed and uncompressed versions of the modeled organ, aiming at comparing also scanners using different breast geometries such as DM and DBT to BCT. In addition, the digital model derived from clinical data helps in reproducing real tissue distribution and the organ silhouette in the devised physical phantoms. Clark et al. (2016) rose concerns related to the use of FDM for manufacturing mammographic phantoms both for the presence of the patterns due to the stratification of the printing processes and for the found low definition of the final phantoms, which resulted unable to reproduce fine details of the breast anatomy also at the light of the high resolution of the DM apparatuses. However, the study of Clark et al. (2016) considered just one FDM printer type and a particular digital model and new technologies may have moderated these aspects. Tests conducted on DM and DBT clinical systems demonstrated that phantoms produced via FDM phantoms permitted to have anatomical noise in the produced images close to that present in clinical images on patient population (Varallo et al., 2022). However, also Varallo et al. (2022) pointed out the presence of artifacts in the produced images that may be ascribed to the printing patterns. In addition, also compatibility of different materials should be tested, hence, the different physical and mechanical properties of these may determine imperfections at the interfaces forming empty spaces in between (Varallo et al., 2022).

Of primary importance is also the selection of the materials used as tissue substitutes. Several authors have evaluated samples made of several materials via SLA, SLS and FDM printers in terms of attenuation coefficients in photon energy ranges usually adopted in 2D and 3D x-ray breast imaging (Ivanov et al., 2018; Santos et al., 2019a; Esposito et al., 2019; Villani et al., 2020; Savi et al., 2021; Mettivier et al., 2022b). The selected materials in the various works were evaluated in terms of attenuation properties and benchmarked versus material usually adopted in the phantom manufacturing – such as PMMA or PE – and versus

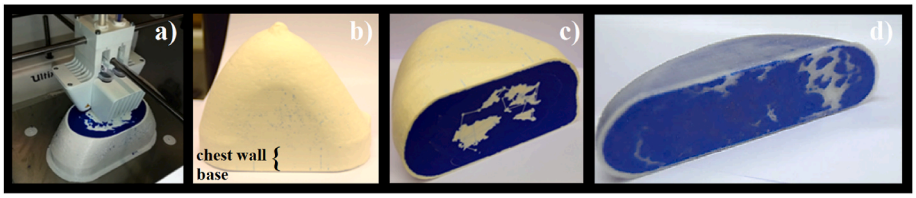

Fig. 7. Examples of compressed anthropomorphic breast phantoms for DM and DMT apparatus testing manufactured with two-extruder FDM technology at the University of Naples (Italy). In these examples, skin and glandular tissue regions were printed with the same material (PLA in a, b and c and PET in d). Adipose regions were reproduced with blue ABS. These images were reproduced from Varallo et al. (2022) with the permission of the publisher.

attenuation coefficients of the tissues. However, these studies were performed for specific printers and printing protocols and no universal validations are acknowledged. Suitability of materials as breast tissues substitute presented also a considerable dependence on the adopted photon energy (Ivanov et al., 2018; Mettivier et al., 2022b).

A promising approach for printing breast phantoms by means of FDM 3D printing technology and one material relies on the use of a variable filament extrusion rate for tuning the density of the printed sample or region (Okkalidis, 2018; Daskalov et al., 2019; Dukov et al., 2022). This approach is meant to overcome the limitation on the number of materials that can be printed at the same time in FDM as well as to avoid problems related to the compatibility of different printing materials. Differently from the conventional printing protocols used with FDM technology, based on a constant rate of the extruded material over the printing session, this innovative approach modifies online the amount of extruded filament per unit time on the basis of the local value of the digital model of the phantom (the breast) producing a variability of the local material density. As second difference from the conventional printing procedure is that the input 3D digital model is the DICOM 3D image whose voxels are expressed in Hounsfield Units (HU), which are directly translated to extrusion rate, avoiding a digital segmented model as for example adopted in other works (di Franco et al., 2019; Varallo et al., 2022). Since the local changes of the object density are meant to produce related local changes in radiodensity of the phantoms, a calibration procedure is performed a priori. This calibration has the main scope of relating the HU to the extrusion rate of the FDM printer for the selected material (Dukov et al., 2022).

In a comparative study to evaluate the most appropriate 3D printing technology for breast phantoms manufacturing, Clark et al. (2016) evidenced that Polyjet overcomes the FDM and SLA technologies in terms of definition of the printed structures due to the high resolution of the DM apparatuses. Polyjet printers build the object layer-by-layer by jetting photopolymer on a tray simultaneously cured by a UV light. However, its advantages come along with an increasing of the cost of both the printer purchasing and the production of a single phantom (Chen et al., 2021). Hence, the cost of Polyjet printer apparatus can reach values more than ~100 times of that of SLA or FDM compact printers (Chen et al., 2021). Similarly, also the cost sustained for the manufacturing of single model via Polyjet printers can reach values up to ~10 times higher than that sustained for SLA; this factor resulted in the order 100 times when Polyjet is compared to FDM (Chen et al., 2021). The high definition of Polyjet 3D printers was exploited for the production of phantoms aiming at producing realistic anatomical noise on the acquired mammograms even with one single material (Badal et al., 2018; Schopphoven et al., 2019; Boita et al., 2021). These phantoms were produced from clinical mammograms whose pixel values were converted into the amount of printing materials with known attenuation coefficient to be put on the x-ray beam path in order to produce a similar signal at the detector plane (Badal et al., 2018). Therefore, from each pixel value was defined the height of a column material focused towards the x-ray focal spot to be included in the built phantom. This approach limits the use of the produced phantoms to the acquisition protocol adopted for the original mammogram (i.e. the same magnification) and it lacks of utility in DBT and BCT 3D imaging with the absence of the replication of the 3D tissue distribution (Badal et al., 2018). Carton et al. (2011) used the Polyjet 3D printer for manufacturing breast phantoms from digital breast models developed at UPenn (Bakic et al., 2002a; 2002b, 2003). They devised a layered phantom replicating the simulated fibroglandular tissue with a material with attenuation properties close to that of 50% glandular breast tissue. Adipose compartments were filled with epoxide-based resin by means of a manual process meant to reduce the presence of air pockets.

Exploiting the PolyJet 3D printing technology, Kiarashi et al. (2015) manufactured breast phantoms starting from digital breast models directly derived from clinical images acquired via a BCT scanner at UC Davis (USA). They outlined two main limitations on the proposed approach: i) the effective spatial resolution permitted by the used 3D printer was larger compared to that of DM and DBT apparatuses and ii) the investigated materials covered a contrast range narrower than that presented by the contrast between adipose and glandular breast tissues. In order to improve the definition of the printed objects, the used printer was manually modified to bypass software control limitations (Sikaria et al., 2016). On the other hand, the selected materials reproduced the attenuation coefficients of breast tissues ranging between 36% and 64% glandular tissues, and alternative solutions to the Doublet phantom manufactured via two materials printed simultaneously (Kiarashi et al., 2015; Ikejimba et al., 2016a) were investigated. Hence, the low attenuation material aimed at reproducing the adipose tissue in the phantoms was substituted with a more appropriate one (Kiarashi et al., 2015). However, this infill process demonstrated to cause air bubbles, which are visible in the radiographic images. The photopolymer producing the highest attenuation coefficient for the printed sample, close to that of 64% was successfully doped with zinc in order to increase the attenuation coefficient to that of 100% glandular tissue (Zhao et al., 2017). In addition, the possibility of adding test details within the anthropomorphic breast phantoms was the most promising application (Zhao et al., 2017; Rossman et al., 2019), this meant to overtake the conventional breast phantoms, with details embedded in homogeneous or quasi-homogenous background (Fig. 8).

With the intent of a summarized comparison, Table 2 reports the main characteristics of the 3D printing technologies here quoted (FDM, SLA, SLS and Polyjet). Due to the large variability of the 3D printer characteristics among different models and producers, information related to the costs are reported in a relative scale.

3.2.2. *Inkjet printed breast phantoms*

Developing physical x-ray breast phantoms by utilizing office inkjet printers is emerging as an easily available and low-cost manufacturing method. The overall scheme of the method involves the usage of off the shelf or inexpensive commercially available inkjet printers, refillable cartridges, paper suitable for printing with the chosen printer and custom-made radiopaque ink. Having obtained the necessary equipment and consumables, the breast phantoms are then fabricated in a slice-by-slice manner, followed by an assembly of the printed sheets to form the 3D object. Most phantoms of this type are limited to mimick adipose and glandular tissues, with few cases where additional objects (lesion, microcalcifications, etc.) are included.

A research group from FDA (Ikejimba et al., 2017a) used a desktop inkjet printer Epson Workforce 630, with a cost of about US$60.00 and refillable cartridges with a cost of around US$4.00 each. Further, for other studies the same group exploited a similar printer type, namely Epson WF-3620 and once more, refillable cartridges (Ikejimba et al., 2019, 2021). Likewise, for the manufacturing of their physical mammography phantom, Manzano-Hernández et al. (2019) used an inexpensive commercially available inkjet printer Epson Stylus CX5900. For printing the phantom, they used one printing cartridge similarly to Georgiev et al. (2021, 2022), who made use of off the shelf low cost inkjet printer HP Officejet 5510.

A key decision in the manufacturing of physical breast phantoms with inkjet printers is the choice of paper. Experimental studies showed that the x-ray attenuation properties of the most types of papers are similar to those of the breast adipose tissue (Ikejimba et al., 2016b, 2017a; Georgiev et al., 2022). Specifically, in Ikejimba et al. (2017a, 2019, 2021) parchment paper with roughly 70 μm thickness was used and studied, with Baking Parchment Paper (King Arthur, Norwich, VT) being chosen as the most appropriate (Ikejimba et al., 2017a). The cost of the paper necessary for a model is reported by the authors to be around US$80. Georgiev et al. (2021, 2022) opted for a plain office paper (80 g m^{-2}) with 100 μm thickness and the paper was deemed successful at mimicking adipose tissue. Similarly, Manzano-Hernández et al. (2019) used Xerox bond paper (75 g m^{-2}) for the recreation of the adipose tissue.

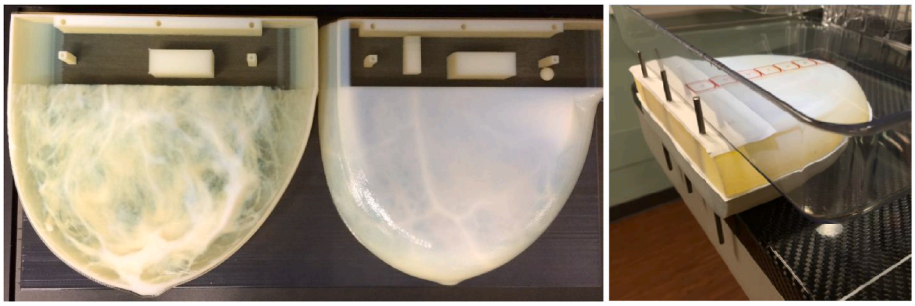

Fig. 8. Doublet phantom manufactured via Polyjet 3D printing technology at Duke University (USA). On the left two half slabs side-by-side with the test details visible on top; on the right the two halves assembled with 3.2 mm diameter titanium rods. Reproduced by Zhao et al. (2017), March, "Third generation anthropomorphic physical phantom for mammography and DBT: Incorporating voxelized 3D printing and uniform chest wall QC region," In Medical Imaging 2017): Physics of Medical Imaging (Vol. 10132, pp. 479–486) SPIE, with the permission of the publisher.

Table 2
Main characteristics of the quoted 3D printing technologies used for breast phantoms manufacturing.

3D printing technology	Commonly used printing layers (mm)	3D printers cost[a]	Cost for manufacturing phantoms[a]	Materials variability	Possibility of producing multi-material phantoms
FDM	0.100–0.400	Very cheap	Very cheap	Large	Yes
SLA	0.025–0.100	Cheap	Moderate	Moderate	No
SLS	0.100–0.120	Moderate	Moderate	Scarce	No
Polyjet	0.014–0.027	Expensive	Very expensive	Moderate	Yes

[a] Data summarized from printers quoted in Chen et al. (2021).

In order to replicate the attenuation properties of the glandular tissue, a custom ink mixture is prepared, which involves the usage of radiopaque substance among others. For the preparation of the glandular ink, Ikejimba et al. (2017a) created a mixture of regular ink (InkThrift) with 350 mg/mL iohexol (Omnipaque), with a price of US $30 for 220 ml of the regular ink and US$200 for 250 ml of the iohexol. Two types of mixtures in that study were reported with solutions of 33% and 25% iohexol by volume. The 33% solution was reported as more attenuating than a glandular tissue, however, with the correct signal difference relative to the parchment paper used as adipose tissue.

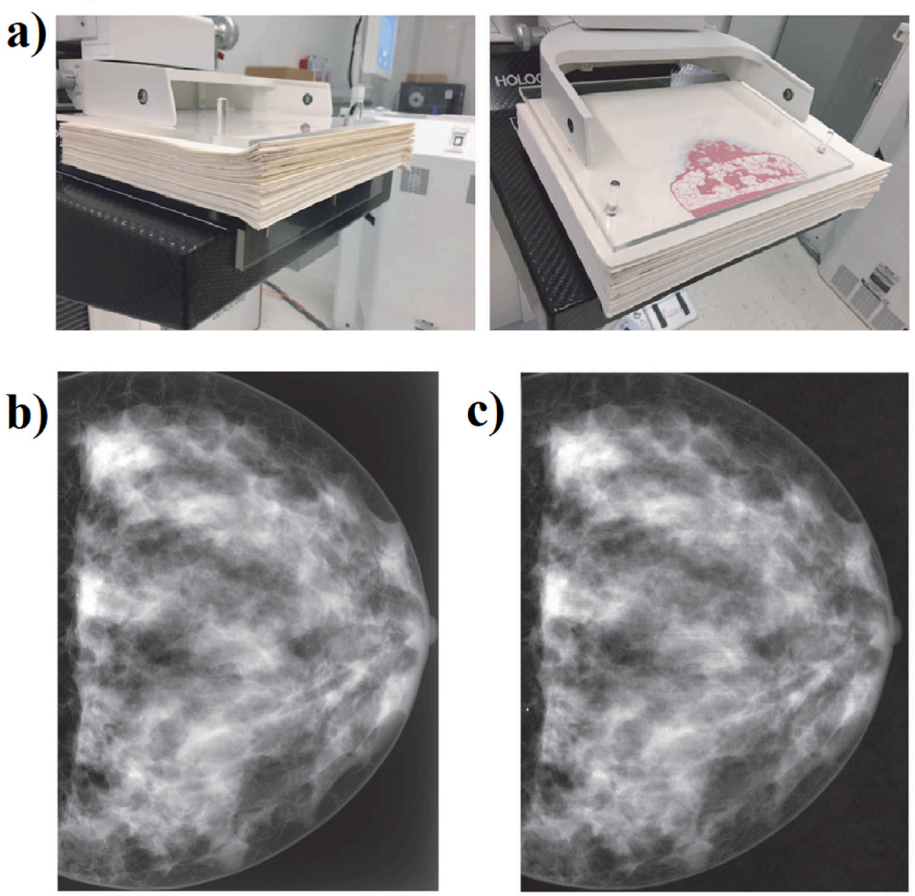

Fig. 9. a) Physical breast phantom created from parchment paper with desktop inkjet printer and iohexol placed on the DM unit. b) Simulated mammogram of the virtual model used for generating the physics phantom and c) acquired DM image of the phantom. Reprinted from (Ikejimba et al., 2017a) with the permission of the publisher.

Manzano-Hernández et al. (2019) on the other hand, mixes black ink (DuraBrite) and Ultravist® 300 contrast medium, with a concentration of 24%. Whereas Georgiev et al. (2021, 2022) created a mixture of 600 mg of potassium iodide (KI) dissolved in 1 ml of water, which was then mixed with standard ink in a 1:1 ratio.

The anthropomorphic phantom created by Ikejimba et al. (2017a, 2019, 2021) was derived from a computational breast model, generated through analytical modeling based in Graff (2016). The printed model is comprised of mimicked adipose and glandular tissues (Ikejimba et al., 2017a); it is shown in Fig. 9, placed between the compression paddle and the support paddle of a DM unit. Comparison between *in-silico* computed DM image of the computational model used for the phantom manufacturing (Fig. 9b) and the planar image of the physical phantom acquired on a clinical DM system (Fig. 9c) showed qualitative similitude. However, fine analysis of the image of the physical phantom outlines some artifacts mainly due to the printing process (Ikejimba et al., 2017a). The inclusion of tumor formations is considered in their work as well. The tumors are computationally generated and in the case of Ikejimba et al. (2017a) they were included after printing the whole model by reprinting the slices containing lesions. For the inclusion of lesions in the physical model, a mixture with higher concentration of iohexol was created in Ikejimba et al. (2021). Furthermore, the highest concentration mixture was placed in a separate color cartridge, thus enabling simultaneous printing of two tissue types. However, with higher concentrations of iohexol the authors reported an increased chance of clogging of the print heads; the dissolvement of KI in water and then mixing it with ink was the proposed approach for overcoming this issue. Ikejimba et al. (2021) included microcalcifications to the phantom as well. The authors created the microcalcifications by crushing tablets made from calcium hydroxyapatite - $Ca_{10}(PO_4)_6(OH)_2$ - and polyvinylpyrrolidone - $(C_6H_9NO)_n$ - powders and sieving the specks. This resulted in objects with sizes between 150 and 180 μm, which were then placed in pre-designed locations. This approach was an improvement over a previous usage of the method reported by the authors in Ikejimba et al. (2019) as well as in Ikejimba et al. (2017a), where crushed eggshells were used. The robustness of the created phantom was tested for a period of over 6 months (Ikejimba et al., 2019). The test consisted of printing four batches with 30 squares with iodine-doped ink on parchment paper, followed by measurements of the attenuation for that period. The data from the measurements were subjected to statistical tests and no statistical significance was found. Reproducibility was also tested and high consistency was reported (Ikejimba et al., 2017a).

While Ikejimba et al. (2017a, 2019, 2021) made use of virtual breast models, Manzano-Hernández et al. (2019) used clinical mammography images, obtained from the American Association of Physics in Medicine (AAPM) Task Group 18 (Samei et al., 2005). The clinical images were processed with a calibration function before printing (Fig. 10). A constraint of the approach is the limited number of gray values that the printer can achieve, namely 256 and the structure of the used paper, which manifests itself as noise in the resulting x-ray images. Nonetheless, satisfactory similarity is reported between the physical phantom x-ray image and the clinical x-ray image, with a Figure of Merit (FOM) of 13% (0% is related to the maximum images similatity). Similarly to Ikejimba et al. (2019), no tendency of loss of contrast was observed for a period of one month.

Georgiev et al. (2021, 2022) produced their model in a similar fashion, with one active printing cartridge. In this case, the data from which the physical breast model was printed is from a segmented clinical breast MRI image set (Dukov et al., 2022). Georgiev et al. (2022) considered two types of tissues: i) adipose tissue replicated by the office paper and ii) glandular tissue denoted by the radiopaque ink. The skin was printed as well, however with the same radiopaque ink created and used for the glandular tissue. The study explored the reproducibility of the phantom and the behavior of the model with different x-ray energies and more precisely with 40 kVp, 60 kVp and 80 kVp. The authors concluded that the technique is reliable and produces realistic results. However, a number of issues are noted, among which clogging due to crystallization of the KI mixture and uncertainty in the KI deposition during printing.

4. Evaluation of innovative materials for breast phantoms manufacturing

Independently of the manufacturing process of an anthropomorphic breast phantom, the choice of the materials to be used for mimicking the human breast anatomy must be adequate to represent the x-ray transmission properties. According to the expected application of the device, these properties and the phantom design may focus on how accurately the material represents the energy deposition of the radiation or the resulting contrast when imaged by DM, DBT or BCT systems. In the first case, the material may be appropriated to dose estimations and in the second case to lead to a realistic representation of the breast image for their quality evaluation. In both cases the choice of the material must consider attributes related to their physical-chemical properties, their adequacy to the prototyping process, reproducibility, spatial resolution, and production costs.

The main physical property to be taken into account for the choice of any tissue-equivalent material (TEM) is the linear attenuation coefficient (LAC) in the range of energies of interest of the specific application. In the case of TEMs for breast-like phantoms, the LAC must be as similar as possible to the breast tissues on the interval of about 5 keV–80 keV, if BCT is considered. If the phantom is planned to be used only for DM or DBT, this range can be limited to 40 keV. Other TEM characterization parameters which impact the photon interactions with a given media

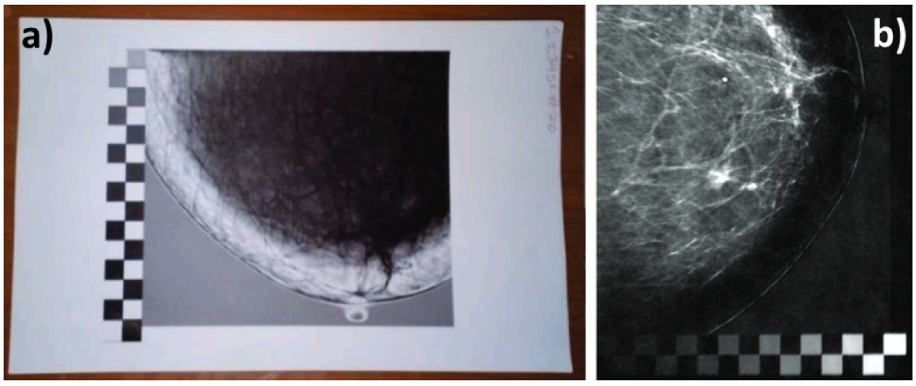

Fig. 10. Physical breast phantom created from bond paper with desktop inkjet printer and contrast medium: a) top view of a paper physical breast model and b) the corresponding mammography image. Reproduced from Manzano-Hernández et al., AIP Conference Proceedings 2090, 030004, (2019); used in accordance with the Creative Commons Attribution (CC BY) license (https://creativecommons.org/licenses/by/4.0/).

have also been recently investigated, such as the effective atomic number, the energy absorption, and the build-up factor (Kadri and Alfuraih, 2022). Therefore, the adequacy of a material used for mimicking real breasts must consider these physical properties, which must be as close as possible to the target-tissue to be modeled. In the case of breast target-tissues, the standard references which provide the elemental composition that allows the comparative evaluations between TEMs and real tissues were published by ICRU (1989), White (1978), Hammerstein et al. (1979) and Johns and Yaffe (1987). Depending on the level of realism expected on the final product, the balance of glandular/adipose components of the breast, which impacts on its dose deposition and imaging aspect, must be also considered. The adequate match between these major components of the breast with the TEM attenuation properties will impact the quality of the phantom. Additionally, if realistic anatomy (Fedon et al., 2021) and/or pathological properties are important, other specific structures must be included on the phantom design in order to reproduce the breast and these designs may be based on computational models or real x-ray images.

Different materials have been introduced in the last years as candidates to representing breast tissues. In a recent review, McGarry et al. (2020) classified the breast phantom design considering their anatomic and non-anatomic properties and presented a complete list of materials that have been considered as TEMs for devising new breast phantoms. In particular, from that review paper, some innovative materials may be highlighted. As also detailed in the previous section, Ikejimba et al. (2017a) produced realistic and inexpensive anthropomorphic phantoms based on an analytical/voxelized model and adopting radiopaque iodine ink into parchment paper as materials associates to an inkjet printer.

Cubukcu and Yucel (2016) implemented an innovative idea, mixing paraffin with two powder additives in order to mimic breast tissues. It is also worth to mention the gelatin-based with tunable x-ray attenuation material reported by Dahal et al. (2018) where the authors mixed gelatin with glycerin in order to remain the material stable and added microbubbles to adequate their attenuation properties. Also very innovative are natural polymer-based hydrogels materials studied by Prabhu et al. (2021) as candidate to TEMs in a broad range of applications, including breast imaging.

As mentioned in sect. 3.2.1, additive manufacturing applied to the construction of anthropomorphic breast phantoms requires not only the development of innovative materials, which is a challenging task, but also creative combinations of regular ones. Two good examples preciously mentioned are the use of paraffin associated to SLA 3D technique by Malliori et al. (2020) and the combination of polyamide-12 and low-viscosity resin by Mainprize et al. (2018, 2020). Polyjet technology associated to UV light curation process was also described in previous section. As presented, the cost limitations of this technology reinforce the importance on investments and research on new materials for application in phantom manufacturing process, as reported by Zhao et al. (2017) and Rossman et al. (2019).

The validation and characterization of any new material introduced as a candidate to TEM is essential to assure the expected response in terms of their physical properties. The most popular method for characterizing these materials used transmission spectrometry to estimate the LAC of a sample of the interest material. The adoption of monochromatic beamlines is the most accurate way to determine these transmission properties, but are expensive and experimentally complex (Ivanov et al., 2018; Esposito et al., 2019; Mettivier et al., 2022b).

Decades ago, similar measurements were published by Byng et al. (1998) using a sophisticated high-purity germanium detector couplet to an electronic system and a multichannel analyzer. These authors determined accurately the linear attenuation coefficients of several commercial TEM used for simulating fat and glandular breast tissues in a range of energies between 10 and 110 keV by employing polyenergetic x-ray beams produced via conventional x-ray tubes. In 2006, Heine and Behera (2006) used a similar method for measuring primary and transmitted spectra using amorphous silicon photodiodes coupled to TFTs and a simple breast phantom. The same approach was used by Ikejimba et al. (2017a) to validate their inkjet-based model.

Recently, the use of cadmium telluride (CdTe) spectrometry technologies became more popular and other TEM characterization experiments were presented in the literature. This kind of detector have been used to characterize clinical mammography x-ray spectra (Santos et al., 2017, 2019b) and it is nowadays a gold standard in terms of x-ray spectrometry in the range of energies for medical imaging applications. Using this kind of detector, a very complete work was proposed by Geraldelli et al. (2013). They applied the Energy Dispersive X-ray technique in different materials, including an adipose-equivalent one. A similar technique was applied by Kabir et al. (2021) using a low energy germanium detector to determine several physical properties of breast TEMs. The previously mentioned works from Cubukcu and Yucel (2016), Badal et al. (2018), Mainprize et al. (2020) and Dahal et al. (2018) also used CdTe detectors for validating their innovative materials. Santos et al. (2019a) used CdTe technique to characterize low-density materials for construction of 3D anthropomorphic breast phantoms. Additional methods for characterization and validation of TEMs include imaging techniques using 2D and 3D mammographic systems (Schopphoven et al., 2019; Dukov et al., 2019a) or CT equipment (Kabir et al., 2021) and the evaluation of effective atomic number and electron density of the materials (Thulasi et al., 2021).

5. Conclusions

The recent literature shows great vivacity in proposing innovative digital and physical breast phantoms. The driving forces conducting the development of new digital phantoms may be found mainly in the need of refining models for x-ray breast dosimetry (AAPM TG282) and in the improved calculation capabilities (i.e. VCT platform based on GPU architectures) which have permitted the development of simulation platform for conducting VCT with reasonable computation times (Badano et al., 2018; Badal et al., 2021; Barufaldi et al., 2018, 2021; Mettivier et al., 2022a). We have identified two major categories of digital breast phantoms: i) those generated from clinical breast images and ii) those obtained by means of mathematical models. Advantages of the first category may be found in the possibility of reproducing the real breast shape and tissue distribution. However, they are mainly derived from images acquired via BCT scanners which implies the limited available cohort (up to now just few thousands of 3D breast images have been acquired with BCT all over the world) and the limits related to the spatial resolution and structure definitions. This last aspect may be a limiting aspect, in particular as regard to the use of such phantoms for VCT in DM and DBT, with the scanners presenting fine spatial resolutions. However, innovative approaches have been proposed to artificially enlarge the phantoms cohort (Sturgeon et al., 2017) and to reduce the voxel sizes and structure definitions in the generated phantoms (Caballo et al., 2018b). It is worth noting that this aspect has shown scarce influence on dosimetric evaluations (Fedon et al., 2018). On the other hand, digital breast phantoms generated from mathematical models permits arbitrary dimension of the voxels and unlimited dimensions of the generated cohorts of digital patients.

Propulsive forces in the development of new physical breast phantoms can be found in the introduction of DBT and BCT in the clinical practice, along with the conventional 2D mammography. Hence, this implied the necessity of developing physical breast phantoms which permitted the evaluation of the image quality of pseudo-3D and 3D imaging systems, whose main advantages reside in the reduction of the tissue superimposition predominant in planar DM imaging. New proposed phantoms have then tended to include the anatomical structure proper of the breast parenchyma, differently from conventional breast phantoms adopted in QA in DM, characterized by the homogeneous background. In this context, 3D printing technologies – which feature the possibility of devising phantoms from (in principle) any digital model – have represented an attempting tool for several research groups

willing to prototype and manufacture their projects. However, SLA and SLS 3D printing technologies have shown their limits related to the possibility of using just one material at a time. This constraint was overtaken with the use of FDM technology either by adopting two extruder printers or the emerging approach which relies on the local variation of the extrusion rate for producing local variation of phantom density (Dukov et al., 2022). Additional features of the FDM technology are related to the large abundance of printing materials, that can be suitably selected for appropriately mimicking the properties of the breast tissues. Main concerns are related to the presence of construction patterns in the manufactured phantoms, that are evident in high resolution images acquired via DM scanners (Varallo et al., 2022). This defect is not present in phantoms printed via Polyjet 3D printing technology, which features the possibility of reproducing fine structures with high spatial resolutions in manufactured objects. The other side of the coin are the large costs of both the printers and the printing materials, as well as the limited number of materials in the case of Polyjet 3D printing. Hence, in most of the cases, these are not able to reproduce the physical properties of the breast tissues and are mixed or tuned by means of conventional material.

Low-cost emerging alternative for manufacturing digital breast phantoms requires the use of inkjet printing on paper with the use of common ink also in conjunction with opportune additive materials. This technique permits to reproduce phantoms whose planar images present anatomical noise comparable to the expected one. However, further studies are needed for the evaluation of their use in 3D imaging.

Declaration of competing interest

The authors declare that they have no known competing financial interests or personal relationships that could have appeared to influence the work reported in this paper.

Data availability

No data was used for the research described in the article.

References

AAPM TG282. Development of a new universal breast dosimetry method, chair I Sechopoulos. https://www.aapm.org/org/structure/?committee_code=tg282.

Abbey, C.K., Bakic, P.R., Pokrajac, D.D., Maidment, A.D.A., Eckstein, M.P., Boone, J.M., 2019. Evaluation of non-Gaussian statistical properties in virtual breast phantoms. J. Med. Imaging 6, 025502.

ACR, 2018. Digital mammography quality control manual - Revised. In: second ed. American College of Radiology May 2020.

Badal, A., Clark, M., Ghammraoui, B., 2018. Reproducing two-dimensional mammograms with three-dimensional printed phantoms. J. Med. Imaging 5, 033501.

Badal, A., Sharma, D., Graff, C.G., Zeng, R., Badano, A., 2021. Mammography and breast tomosynthesis simulator for virtual clinical trials. Comput. Phys. Commun. 261, 107779.

Badano, A., 2021. In silico imaging clinical trials: cheaper, faster, better, safer, and more scalable. Trials 22, 1–7.

Badano, A., Badal, A., Glick, S., Graff, C.G., Samuelson, F., Sharma, D., Zeng, R.P., 2017. In silico imaging clinical trials for regulatory evaluation: initial considerations for VICTRE, a demonstration study. In: Flohr, T.G., Lo, J.Y., Schmidt, T.G. (Eds.), Medical Imaging 2017: Physics of Medical Imaging, vol. 10132. Spie-Int Soc Optical Engineering, Bellingham.

Badano, A., Graff, C.G., Badal, A., Sharma, D., Zeng, R., Samuelson, F.W., et al., 2018. Evaluation of digital breast tomosynthesis as replacement of full-field digital mammography using an in silico imaging trial. JAMA Netw. Open 1 (7) e185474-e185474.

Bakic, P.R., Albert, M., Brzakovic, D., Maidment, A.D.A., 2002a. Mammogram synthesis using a 3D simulation. I. Breast tissue model and image acquisition simulation. Med. Phys. 29, 2131–2139.

Bakic, P.R., Albert, M., Brzakovic, D., Maidment, A.D.A., 2002b. Mammogram synthesis using a 3D simulation. II. Evaluation of synthetic mammogram texture. Med. Phys. 29, 2140–2151.

Bakic, P.R., Albert, M., Brzakovic, D., Maidment, A.D.A., 2003. Mammogram synthesis using a three-dimensional simulation. III. Modeling and evaluation of the breast ductal network. Med. Phys. 30, 1914–1925.

Bakic, P.R., Zhang, C.P., Maidment, A.D.A., 2011. Development and characterization of an anthropomorphic breast software phantom based upon region-growing algorithm. Med. Phys. 38, 3165–3176.

Bakic, P.R., Barufaldi, B., Higginbotham, D., Weinstein, S.P., Avanaki, A.N., Espig, K.S., Xthona, A., Kimpe, T.R.L., Maidment, A.D.A., 2018a. Virtual clinical trial of lesion detection in digital mammography and digital breast tomosynthesis. In: Conference on Medical Imaging - Physics of Medical Imaging. Feb 12-15, Houston, TX.

Bakic, P.R., Barufaldi, B., Pokrajac, D.D., Weinstein, S.P., Maidment, A.D.A., 2018b. Optimized simulation of breast anatomy for virtual clinical trials. In: 14th International Workshop on Breast Imaging (IWBI). Emory Univ, Atlanta, GA. Jul 08-11.

Barufaldi, B., Higginbotham, D., Bakic, P.R., Maidment, A.D.A., 2018. OpenVCT: a GPU-accelerated virtual clinical trial pipeline for mammography and digital breast tomosynthesis. In: Conference on Medical Imaging - Physics of Medical Imaging. Feb 12-15, Houston, TX.

Barufaldi, B., Vent, T.L., Acciavatti, R.J., Bakic, P.R., Noel, P.B., Conant, E.F., Maidment, A.D.A., 2020. Determining the optimal angular range of the X-ray source motion in tomosynthesis using virtual clinical trials. In: Conference on Medical Imaging - Physics of Medical Imaging. Feb 16-19, Houston, TX.

Barufaldi, B., Maidment, A.D., Dustler, M., Axelsson, R., Tomic, H., Zackrisson, S., et al., 2021. Virtual clinical trials in medical imaging system evaluation and optimisation. Radiat. Protect. Dosim. 195, 363–371.

Barufaldi, B., Vent, T.L., Bakic, P.R., Maidment, A.D.A., 2022. Computer simulations of case difficulty in digital breast tomosynthesis using virtual clinical trials. Med. Phys. 49, 2220–2232.

Bliznakova, K., 2016. The use of 3D printing in manufacturing anthropomorphic phantoms for biomedical applications. Scripta Scientifica Medicinae Dentalis 2, 23–31.

Bliznakova, K., 2020. The advent of anthropomorphic three-dimensional breast phantoms for X-ray imaging. Phys. Med. 79, 145–161.

Bliznakova, K., Bliznakov, Z., Bravou, V., Kolitsi, Z., Pallikarakis, N., 2003. A three-dimensional breast software phantom for mammography simulation. Phys. Med. Biol. 48, 3699–3719.

Bliznakova, K., Suryanarayanan, S., Karellas, A., Pallikarakis, N., 2010. Evaluation of an improved algorithm for producing realistic 3D breast software phantoms: application for mammography. Med. Phys. 37, 5604–5617.

Bliznakova, K., Sechopoulos, I., Buliev, I., Pallikarakis, N., 2012. BreastSimulator: a software platform for breast x-ray imaging research. J. Biomed. Graph. Comput. 2, 1.

Bliznakova, K., Dukov, N., Feradov, F., Gospodinova, G., Bliznakov, Z., Russo, P., et al., 2019. Development of breast lesions models database. Phys. Med. 64, 293–303.

Bliznakova, K., Okkalidis, N., Sarno, A., Dukov, N., Mettivier, G., Russo, P., Bliznakov, Z., 2020. Physical anthropomorphic breast phantoms for X-ray imaging techniques: manufacturing approach. In: 2020 International Conference on E-Health and Bioengineering (EHB). IEEE, pp. 1–4.

Boita, J., Mackenzie, A., van Engen, R.E., Broeders, M., Sechopoulos, I., 2021. Validation of a mammographic image quality modification algorithm using 3D-printed breast phantoms. J. Med. Imaging 8, 033502.

Boone, J.M., Hernandez, A.M., Seibert, J.A., 2017. Two-dimensional breast dosimetry improved using three-dimensional breast image data. Radiological physics and technology 10, 129–141.

Borges, L.R., Barufaldi, B., Caron, R.F., Bakic, P.R., Foi, A., Maidment, A.D.A., Vieira, M. A.C., 2019. Technical Note: noise models for virtual clinical trials of digital breast tomosynthesis. Med. Phys. 46, 2683–2689.

Bouwman, R.W., Van Engen, R.E., Young, K.C., Den Heeten, G.J., Broeders, M.J.M., Schopphoven, S., et al., 2015. Average glandular dose in digital mammography and digital breast tomosynthesis: comparison of phantom and patient data. Phys. Med. Biol. 60, 7893–7907.

Brombal, L., Arfelli, F., Delogu, P., Donato, S., Mettivier, G., Michielsen, K., et al., 2019. Image quality comparison between a phase-contrast synchrotron radiation breast CT and a clinical breast CT: a phantom based study. Sci. Rep. 9, 1–12.

Byng, J.W., Mainprize, J.G., Yaffe, M.-J., 1998. X-ray characterization of breast phantom materials. Phys. Med. Biol. 43, 1367–1377.

Caballo, M., Boone, J.M., Mann, R., Sechopoulos, I., 2018a. An unsupervised automatic segmentation algorithm for breast tissue classification of dedicated breast computed tomography images. Med, Phys. 45, 2542–2559.

Caballo, M., Fedon, C., Brombal, L., Mann, R., Longo, R., Sechopoulos, I., 2018b. Development of 3D patient-based super-resolution digital breast phantoms using machine learning. Phys. Med. Biol. 63, 225017.

Caballo, M., Rabin, C., Fedon, C., Rodriguez-Ruiz, A., Diaz, O., Boone, J.M., Dance, D.R., Sechopoulos, I., 2022. Patient-derived heterogeneous breast phantoms for advanced dosimetry in mammography and tomosynthesis. Med. Phys. 49, 5423–5438.

Carton, A.K., Bakic, P., Ullberg, C., Derand, H., Maidment, A.D.A., 2011. Development of a physical 3D anthropomorphic breast phantom. Med. Phys. 38, 891–896.

Chen, L., Abbey, C.K., Nosratieh, A., Lindfors, K.K., Boone, J.M., 2012. Anatomical complexity in breast parenchyma and its implications for optimal breast imaging strategies. Med. Phys 39, 1435–1441.

Chen, L., Craig, K.A., Boone, J.M., 2013. Association between power law coefficients of the anatomical noise power spectrum and lesion detectability in breast imaging modalities. Phys. Med. Biol. 58, 1663–1681.

Chen, J.V., Dang, A.B., Dang, A., 2021. Comparing cost and print time estimates for six commercially-available 3D printers obtained through slicing software for clinically relevant anatomical models. 3D Print. Med. 7, 1–14.

Clark, M., Ghammraoui, B., Badal, A., 2016. Reproducing 2D breast mammography images with 3D printed phantoms. In: Medical Imaging 2016: Physics of Medical Imaging, vol. 9783, pp. 89–97 (SPIE).

Cockmartin, L., Bosmans, H., Marshall, N.W., 2013. Comparative power law analysis of structured breast phantom and patient images in digital mammography and breast tomosynthesis. Med. Phys. 40, 081920.
Cockmartin, L., Marshall, N.W., Van Ongeval, C., Aerts, G., Stalmans, D., Zanca, F., et al., 2015. Comparison of digital breast tomosynthesis and 2D digital mammography using a hybrid performance test. Phys. Med. Biol. 60, 3939.
Cockmartin, L., Marshall, N.W., Zhang, G., Lemmens, K., Shaheen, E., Van Ongeval, C., et al., 2017. Design and application of a structured phantom for detection performance comparison between breast tomosynthesis and digital mammography. Phys. Med. Biol. 62, 758.
Cubukcu, S., Yucel, H., 2016. Characterization of paraffin based breast tissue equivalent phantom using a CdTe detector pulse height analysis. Australas. Phys. Eng. Sci. Med. 39, 877–884.
Dahal, E., Badal, A., Zidan, A., Alayoubi, A., Hagio, T., Glick, S., Badano, A., Ghammraoui, B., 2018. Stable gelatin-based phantom materials with tunable x-ray attenuation properties and 3D printability for x-ray imaging. Phys. Med. Biol. 63, 09NT01.
Dance, D.R., Sechopoulos, I., 2016. Dosimetry in x-ray-based breast imaging. Phys. Med. Biol. 61, R271.
Dance, D.R., Skinner, C.L., Young, K.C., Beckett, J.R., Kotre, C.J., 2000. Additional factors for the estimation of mean glandular breast dose using the UK mammography dosimetry protocol. Phys. Med. Biol. 45, 3225–3240. https://doi.org/10.1088/0031-9155/45/11/308.PMID:11098900.
Dance, D.R., Young, K.C., Van Engen, R.E., 2010. Estimation of mean glandular dose for breast tomosynthesis: factors for use with the UK, European and IAEA breast dosimetry protocols. Phys. Med. Biol. 56, 453–471.
Daskalov, S., Okkalidis, N., Boone, J.M., Marinov, S., Bliznakov, Z., Mettivier, G., et al., 2019. Anthropomorphic physical breast phantom based on patient breast CT data: preliminary results. In: Mediterranean Conference on Medical and Biological Engineering and Computing. Springer, Cham, pp. 367–374.
de las Heras, H., Schöfer, F., Tiller, B., Chevalier, M., Zwettler, G., Semturs, F., 2013. A phantom using titanium and Landolt rings for image quality evaluation in mammography. Phys. Med. Biol. 58, L17.
di Franco, F., Mettivier, G., Sarno, A., Varallo, A., Russo, P., 2019. Manufacturing of physical breast phantoms with 3D printing technology for X-ray breast imaging. In: 2019 IEEE Nuclear Science Symposium and Medical Imaging Conference. NSS/MIC), pp. 1–5 (IEEE).
di Franco, F., Sarno, A., Mettivier, G., Hernandez, A.M., Bliznakova, K., Boone, J.M., Russo, P., 2020. GEANT4 Monte Carlo simulations for virtual clinical trials in breast X-ray imaging: proof of concept. Phys. Med. 74, 133–142.
Dukov, N., Bliznakova, K., Feradov, F., Ridlev, I., Bosmans, H., Mettivier, G., Russo, P., Cockmartin, L., Bliznakov, Z., 2019a. Models of breast lesions based on three-dimensional X-ray breast images. Phys. Med. 57, 80–87.
Dukov, N.T., Feradov, F.N., Gospodinova, G.D., Bliznakova, K.S., 2019b. An approach for printing tissue-mimicking abnormalities dedicated to applications in breast imaging. In: 2019 IEEE XXVIII International Scientific Conference Electronics (ET). IEEE, pp. 1–4.
Dukov, N., Bliznakova, K., Teneva, T., Marinov, S., Bakic, P., Bosmans, H., Bliznakov, Z., 2020. Experimental evaluation of physical breast phantoms for 2D and 3D breast x-ray imaging techniques. In: European Medical and Biological Engineering Conference. Springer, Cham, pp. 544–552.
Dukov, N., Bliznakova, K., Okkalidis, N., Teneva, T., Encheva, E., Bliznakov, Z., 2022. Thermoplastic 3D printing technology using a single filament for producing realistic patient-derived breast models. Phys. Med. Biol. 67, 045008.
EFOMP, 2015. Quality controls in digital mammography, protocol of the EFOMP mammo working group. https://www.efomp.org.
Elangovan, P., Mackenzie, A., Dance, D.R., Young, K.C., Cooke, V., Wilkinson, L., Given-Wilson, R.M., Wallis, M.G., Wells, K., 2017. Design and validation of realistic breast models for use in multiple alternative forced choice virtual clinical trials. Phys. Med. Biol. 62, 2778–2794.
Erickson, D.W., Wells, J.R., Sturgeon, G.M., Samei, E., Dobbins III, J.T., Segars, W.P., Lo, J.Y., 2016. Population of 224 realistic human subject-based computational breast phantoms. Med. Phys. 43, 23–32.
Esposito, G., Mettivier, G., Bliznakova, K., Bliznakov, Z., Bosmans, H., Bravin, A., et al., 2019. Investigation of the refractive index decrement of 3D printing materials for manufacturing breast phantoms for phase contrast imaging. Phys. Med. Biol. 64, 075008.
EUREF, 2006. 4th edition of the European guidelines for quality assurance in breast cancer screening and diagnosis. http://euref.org/european-Guidelines.
EUREF, 2018. Protocol for the Quality Control of the Physical and Technical Aspects of Digital Breast Tomosynthesis Systems version 1.03. https://euref.org/european-guidelines/physico-technical-protocol#breasttomo.
Fedon, C., Rabin, C., Caballo, M., Diaz, O., García, E., Rodríguez-Ruiz, A., et al., 2018. Monte Carlo study on optimal breast voxel resolution for dosimetry estimates in digital breast tomosynthesis. Phys. Med. Biol. 64, 015003.
Fedon, C., Van Engen, R., Binst, J., Cockmartin, L., Dance, D.R., et al., 2019. B-1838: Proposal of a Breast Phantom for Dosimetry Quality Control Procedures in Digital Mammography and Digital Breast Tomosynthesis ECR2019 Book of Abstract. European Congress of Radiology 2019, Vienna, Austria. February 27 - March 3, 2019).
Fedon, C., Caballo, M., García, E., Diaz, O., Boone, J.M., Dance, D.R., Sechopoulos, I., 2021. Fibroglandular tissue distribution in the breast during mammography and tomosynthesis based on breast CT data: a patient-based characterization of the breast parenchyma. Med. Phys. 48, 1436–1447.
Feradov, F., Marinov, S., Bliznakova, K., 2019. Physical Breast Phantom Dedicated for Mammography Studies. 15th Mediterranean Conference on Medical and Biological Engineering and Computing (MEDICON), Sep 26-28. UNESCO World Heritage Univ, Coimbra, PORTUGAL, pp. 344–352.
Gang, G.J., Tward, D.J., Lee, J., Siewerdsen, J.H., 2010. Anatomical background and generalized detectability in tomosynthesis and cone-beam CT. Med. Phys. 37, 1948–1965.
Garcia, E., Fedon, C., Caballo, M., Marti, R., Sechopoulos, I., Diaz, O., 2020. Realistic compressed breast phantoms for medical physics applications. In: 15th International Workshop on Breast Imaging (IWBI). Electr Network. May 25-27.
Gazi, P.M., Yang, K., Burkett Jr., G.W., Aminololama-Shakeri, S., Seibert, A.J., Boone, J. M., 2015. Evolution of spatial resolution in breast CT at UC Davis. Med. Phys. 42, 1973–1981.
Geiser, W.R., Einstein, S.A., Yang, W.T., 2018. Artifacts in digital breast tomosynthesis. Am. J. Roentgenol. 211, 926–932.
Georgiev, T., Bliznakova, K., Kolev, I., Dukov, N., Bliznakov, Z., 2020. An approach for development of a physical breast phantom for X-ray imaging using an inkjet printer: preliminary results. In: The International Symposium on Bioinformatics and Biomedicine. Springer, Cham, pp. 384–389.
Georgiev, T.P., Kolev, I., Dukov, N., Mavrodinova, S., Yordanova, M., Bliznakova, K., 2021. Development of an inkjet calibration phantom for x-ray imaging studies. Scripta Scientifica Medica 53, 15–20. https://doi.org/10.14748/ssm.v0i0.7410.
Georgiev, T., Bliznakova, K., Kolev, I., Dukov, N., Bliznakov, Z., 2022. An approach for development of a physical breast phantom for X-ray imaging using an inkjet printer: preliminary results. In: Sotirov, S.S., Pencheva, T., Kacprzyk, J., Atanassov, K.T., Sotirova, E., Staneva, G. (Eds.), Contemporary Methods in Bioinformatics and Biomedicine and Their Applications, Lecture Notes in Networks and Systems. Springer International Publishing, Cham, pp. 384–389. https://doi.org/10.1007/978-3-030-96638-6_40.
Geraldelli, W., Tomal, A., Poletti, M.E., 2013. Characterization of tissue-equivalent materials through measurements of the linear attenuation coefficient and scattering profiles obtained with Polyenergetic Beams. IEEE Trans. Nucl. Sci. 60, 566–571.
Germann, M., Shim, S., Angst, F., Saltybaeva, N., Boss, A., 2021. Spiral breast computed tomography (CT): signal-to-noise and dose optimization using 3D-printed phantoms. Eur. Radiol. 31, 3693–3702.
Glick, S.J., Ikejimba, L.C., 2018. Advances in digital and physical anthropomorphic breast phantoms for x-ray imaging. Med. Phys. 45, e870–e885.
Graff, C.G., 2016. A new, open-source, multi-modality digital breast phantom. In: Conference on Medical Imaging - Physics of Medical Imaging. Feb 28-Mar 02, San Diego, CA.
Hammerstein, G.R., Miller, D.W., White, D.R., Masterson, M.E., Woodard, H.Q., Laughlin, J.S., 1979. Absorbed radiation dose in mammography. Radiology 130, 485–491.
He, Y., Liu, Y., Dyer, B.A., Boone, J.M., Liu, S., Chen, T., et al., 2019. 3D-printed breast phantom for multi-purpose and multi-modality imaging. Quant. Imag. Med. Surg. 9, 63.
Heine, J.J., Behera, M., 2006. Effective x-ray attenuation measurements with full field digital mammography. Med. Phys. 33, 4350–4366.
Hernandez, A.M., Seibert, J.A., Boone, J.M., 2015. Breast dose in mammography is about 30% lower when realistic heterogeneous glandular distributions are considered. Med. Phys. 42, 6337–6348.
Hsu, C.M., Palmeri, M.L., Segars, W.P., Veress, A.I., Dobbins III, J.T., 2013. Generation of a suite of 3D computer-generated breast phantoms from a limited set of human subject data. Med. Phys. 40, 043703.
Huang, S.Y., Boone, J.M., Yang, K., Kwan, A.L., Packard, N.J., 2008. The effect of skin thickness determined using breast CT on mammographic dosimetry. Med. Phys. 35, 1199–1206.
Huang, S.Y., Boone, J.M., Yang, K., Packard, N.J., McKenney, S.E., Prionas, N.D., eta, al, 2011. The characterization of breast anatomical metrics using dedicated breast CT. Med. Phys. 38, 2180–2191.
IAEA, 2011. Human Health Series No. 17 Quality assurance programme for digital mammography. Wien. https://iaea.org/publications/8560/quality-assurance-programme-for-digital-mammography.
ICRU, 1989. Tissue substitutes in radiation dosimetry and measurement (ICRU report No. 44). International Commission on Radiation Units and Measurements.
Ikejimba, L.C., Kiarashi, N., Ghate, S.V., Samei, E., Lo, J.Y., 2014. Task-based strategy for optimized contrast enhanced breast imaging: analysis of six imaging techniques for mammography and tomosynthesis. Med. Phys. 41, 061908.
Ikejimba, L.C., Lo, J.Y., Chen, Y., Oberhofer, N., Kiarashi, N., Samei, E., 2016a. A quantitative metrology for performance characterization of five breast tomosynthesis systems based on an anthropomorphic phantom. Med. Phys. 43, 1627–1638.
Ikejimba, L., Graff, C., Glick, S., 2016b. Rapid generation of structured physical phantoms for mammography and digital breast tomosynthesis. In: Tingberg, A., Lång, K., Timberg, P. (Eds.), Breast Imaging, Lecture Notes in Computer Science. Springer International Publishing, Cham, pp. 654–659. https://doi.org/10.1007/978-3-319-41546-8_81.
Ikejimba, L.C., Graff, C.G., Rosenthal, S., Badal, A., Ghammraoui, B., Lo, J.Y., Glick, S.J., 2017a. A novel physical anthropomorphic breast phantom for 2D and 3D x-ray imaging. Med. Phys. 44, 407–416.
Ikejimba, L.C., Graff, C.G., Rosenthal, S., Badal, A., Ghammraoui, B., Lo, J.Y., Glick, S.J., 2017b. A physical breast phantom for 2D and 3D x-ray imaging made through inkjet printing. In: Flohr, T.G., Lo, J.Y., Schmidt, T.G. (Eds.), Medical Imaging 2017: Physics of Medical Imaging, vol. 10132. Spie-Int Soc Optical Engineering, Bellingham.
Ikejimba, L.C., Salad, J., Graff, C.G., Ghammraoui, B., Cheng, W.-C., Lo, J.Y., Glick, S.J., 2019. A four-alternative forced choice (4AFC) methodology for evaluating microcalcification detection in clinical full-field digital mammography (FFDM) and

digital breast tomosynthesis (DBT) systems using an inkjet-printed anthropomorphic phantom. Med. Phys. 46, 3883–3892. https://doi.org/10.1002/mp.13629.
Ikejimba, L.C., Salad, J., Graff, C.G., Goodsitt, M., Chan, H.-P., Huang, H., Zhao, W., Ghammraoui, B., Lo, J.Y., Glick, S.J., 2021. Assessment of task-based performance from five clinical DBT systems using an anthropomorphic breast phantom. Med. Phys. 48, 1026–1038. https://doi.org/10.1002/mp.14568.
IPEM, 2005. Institute of Physics and Engineering in Medicine. The commissioning and routine testing of mammographic x-ray systems IPEM Report 89 York, United Kingdom (IPEM).
Ivanov, D., Bliznakova, K., Buliev, I., Popov, P., Mettivier, G., Russo, P., et al., 2018. Suitability of low density materials for 3D printing of physical breast phantoms. Phys. Med. Biol. 63, 175020.
Johns, P.C., Yaffe, M.J., 1987. X-ray characterisation of normal and neoplastic breast tissues. Phys. Med. Biol. 32, 675.
Kabir, N.A., Okoh, F.O., Mohd Yusof, M.F., 2021. Radiological and physical properties of tissue equivalent mammography phantom: characterization and analysis methods. Radiat. Phys. Chem. 180, 109271.
Kadri, O., Alfuraih, A., 2022. Search for tissue equivalent materials based on exposure and energy absorption buildup factor computations. Appl. Sci. 12, 798.
Karssemeijer, N., Thijssen, M.A.O., 1996. Determination of contrast-detail curves of mammography systems by automated image analysis. Digital Mammography '96. Proceedings of the 3rd International Workshop on Digital Mammography 155–160.
Kiarashi, N., Nolte, A.C., Sturgeon, G.M., Segars, W.P., Ghate, S.V., Nolte, L.W., et al., 2015. Development of realistic physical breast phantoms matched to virtual breast phantoms based on human subject data. Med. Phys. 42, 4116–4126.
Klausz, R., Rouxel, M., Mancardi, X., Carton, A.K., Patoureaux, F.J., 2018. Introduction of a Comprehensive Phantom for the Quality Control of Contrast Enhanced Spectral Mammography. European Congress of Radiology-ECR, 2018.
Kuttig, J.D., Steiding, C., Kolditz, D., Hupfer, M., Karolczak, M., Kalender, W.A., 2015. Comparative investigation of the detective quantum efficiency of direct and indirect conversion detector technologies in dedicated breast CT. Phys. Med. 31, 406–413.
Lau, B.A., Reiser, I., Nishikawa, R.M., Bakic, P.R., 2012. A statistically defined anthropomorphic software breast phantom. Med. Phys. 39, 3375–3385.
Li, C.M., Segars, W.P., Tourassi, G.D., Boone, J.M., Dobbins, J.T., 2009. Methodology for generating a 3D computerized breast phantom from empirical data. Med. Phys. 36, 3122–3131.
Longo, R., Arfelli, F., Bonazza, D., Bottigli, U., Brombal, L., Contillo, A., et al., 2019. Advancements towards the implementation of clinical phase-contrast breast computed tomography at Elettra. J. Synchrotron Radiat. 26, 1343–1353.
Ma, A.K.W., Gunn, S., Darambara, D.G., 2009. Introducing DeBRa: a detailed breast model for radiological studies. Phys. Med. Biol. 54, 4533–4545.
Mahr, D.M., Bhargava, R., Insana, M.F., 2012. Three-Dimensional in silico breast phantoms for multimodal image simulations. Ieee Trans. Med. Im. 31, 689–697.
Maidment, A., Bakic, P., Barufaldi, B., 2018. What limits the detection of calcifications in tomosynthesis. Med. Phys. 45 (6). E518-E518.
Mainprize, J.G., Carton, A.K., Klausz, R., Li, Z., Hunter, D.M., Mawdsley, G.E., Muller, S., Yaffe, M.J., 2018. Development of a Physical 3D Anthropomorphic Breast Texture Model Using Selective Laser Sintering Rapid Prototype Printing SPIE 10573, p. 105730A.
Mainprize, J.G., Mawdsley, G.E., Carton, A.K., Li, Z., Klausz, R., Muller, S., Yaffe, M.J., 2020. Full-size Anthropomorphic Phantom for 2D and 3D Breast X-Ray Imaging SPIE 11513, 1151302.
Malliori, A., Bliznakova, K., Sechopoulos, I., Kamarianakis, Z., Fei, B., Pallikarakis, N., 2014. Breast tomosynthesis with monochromatic beams: a feasibility study using Monte Carlo simulations. Phys. Med. Biol. 59, 4681–4696.
Malliori, A., Daskalaki, A., Dermitzakis, A., Pallikarakis, N., 2020. Development of physical breast phantoms for X-ray imaging employing 3D printing techniques. Open Med. Imag. J. 12 (1).
Manzano-Hernández, J.R., López-Pineda, E., Brandan, M.-E., 2019. Generation of a mammographic phantom using an inkjet printer and radiopaque ink. AIP Conf. Proc. 2090, 030004 https://doi.org/10.1063/1.5095899.
Marshall, N.W., Bosmans, H., 2022. Performance evaluation of digital breast tomosynthesis systems: comparison of current virtual clinical trial methods. Phys. Med. Biol 67, 22TR03.
Massera, R.T., Tomal, A., 2018. Skin models and their impact on mean glandular dose in mammography. Phys. Med. 51, 38–47.
McGarry, C.K., Grattan, L.J., Ivory, A.M., Leek, F., Liney, G.P., Liu, Y., Miloro, P., Rai, R., Robinson, A., Shih, A.J., Zeqiri, B., Clark, C.H., 2020. Tissue mimicking materials for imaging and therapy phantoms: a review. Phys. Med. Biol. 62, 23TR01.
Mettivier, G., Bliznakova, K., Di Lillo, F., Sarno, A., Russo, P., 2016. Evaluation of the BreastSimulator software platform for breast tomography: preliminary results. In: 13th International Workshop on Breast Imaging (IWDM), pp. 145–151. Jun 19-22, Malmo, SWEDEN.
Mettivier, G., Bliznakova, K., Sechopoulos, I., Boone, J.M., Di Lillo, F., Sarno, A., Castriconi, R., Russo, P., 2017. Evaluation of the BreastSimulator software platform for breast tomography. Phys. Med. Biol. 62, 6446–6466.
Mettivier, G., Sarno, A., Boone, J.M., Bliznakova, K., di Franco, F., Russo, P., 2020. Virtual clinical trials in 3D and 2D breast imaging with digital phantoms derived from clinical breast CT scans. In: Conference on Medical Imaging - Physics of Medical Imaging. Feb 16-19, Houston, TX.
Mettivier, G., Sarno, A., Lai, Y., Golosio, B., Fanti, V., Italiano, M.E., et al., 2022a. Virtual clinical trials in 2D and 3D X-ray breast imaging and dosimetry: comparison of CPU-based and GPU-based Monte Carlo codes. Cancers 14, 1027.
Mettivier, G., Sarno, A., Varallo, A., Russo, P., 2022b. Attenuation coefficient in the energy range 14−36 keV of 3D printing materials for physical breast phantoms. Phys. Med. Biol. 67, 175012.
NHS, 2009. NHS Breast Screening Programme Equipment Report 0604 Version 3 COMMISSIONING and ROUTINE TESTING of FULL FIELD DIGITAL MAMMOGRAPHY SYSTEMS April 2009.
NHS, 2015. NHS Breast Screening Programme Equipment Report 1407 Routine Quality Control Tests for Breast Tomosynthesis (Physicists) December 2015.
Niklason, L.T., Christian, B.T., Niklason, L.E., Kopans, D.B., Castleberry, D.E., Opsahl-Ong, B.H., et al., 1997. Digital tomosynthesis in breast imaging. Radiology 205, 399–406.
Okkalidis, N., 2018. A novel 3D printing method for accurate anatomy replication in patient-specific phantoms. Med. Phys. 45, 4600–4606.
Pokrajac, D.D., Maidment, A.D.A., Bakic, P.R., 2012. Optimized generation of high resolution breast anthropomorphic software phantoms. Med. Phys. 39, 2290–2302.
Prabhu, S., Bharadwaj, D.Y., Podder, R., Bubbly, S.G., Gudennavar, S.B., 2021. Natural polymer-based hydrogels as prospective tissue equivalent materials for radiation therapy and dosimetry. Phys. Eng. Sci. Med. 44, 1107–1120.
Rossman, A.H., Catenacci, M., Zhao, C., Sikaria, D., Knudsen, J.E., Dawes, D., et al., 2019. Three-dimensionally-printed anthropomorphic physical phantom for mammography and digital breast tomosynthesis with custom materials, lesions, and uniform quality control region. J. Med. Imaging 6, 021604.
Samei, E., Badano, A., Chakraborty, D., Compton, K., Cornelius, C., Corrigan, K., Flynn, M.J., et al., 2005. Assessment of display performance for medical imaging systems: executive summary of AAPM TG18 report. Med. Phys. 32, 1205–1225. https://doi.org/10.1118/1.1861159.
Santos, J.C., Tomal, A., Furquim, T.A., Fausto, A.M.F., Nogueira, M.S., Costa, P.R., 2017. Direct measurement of clinical mammographic x-ray spectra using a CdTe spectrometer. Med. Phys. 44, 3504–3511.
Santos, J.C., Almeida, C.D., Iwahara, A., Peixoto, J.E., 2019a. Characterization and applicability of low-density materials for making 3D physical anthropomorphic breast phantoms. Radiat. Phys. Chem. 164, 108361.
Santos, J.C., Tomal, A., de Barros, N., Costa, P.R., 2019b. Normalized glandular dose (DgN) coefficients from experimental mammographic x-ray spectra. Phys. Med. Biol. 64, 105010.
Sarno, A., Mettivier, G., Russo, P., 2015. Dedicated breast computed tomography: basic aspects. Med. Phys. 42, 2786–2804.
Sarno, A., Mettivier, G., Golosio, B., Oliva, P., Spandre, G., Di Lillo, F., et al., 2016a. Imaging performance of phase-contrast breast computed tomography with synchrotron radiation and a CdTe photon-counting detector. Phys. Med. 32, 681–690.
Sarno, A., Mettivier, G., Di Lillo, F., Russo, P., 2016b. A Monte Carlo study of monoenergetic and polyenergetic normalized glandular dose (DgN) coefficients in mammography. Phys. Med. Biol. 62, 306.
Sarno, A., Dance, D.R., Van Engen, R.E., Young, K.C., Russo, P., Di Lillo, F., et al., 2017. A Monte Carlo model for mean glandular dose evaluation in spot compression mammography. Med. Phys. 44, 3848–3860.
Sarno, A., Mettivier, G., Di Lillo, F., Bliznakova, K., Sechopoulos, I., Russo, P., 2018a. Homogeneous vs. patient specific breast models for Monte Carlo evaluation of mean glandular dose in mammography. Phys. Med. 51, 56–63.
Sarno, A., Mettivier, G., Tucciariello, R.M., Bliznakova, K., Boone, J.M., Sechopoulos, I., et al., 2018b. Monte Carlo evaluation of glandular dose in cone-beam X-ray computed tomography dedicated to the breast: homogeneous and heterogeneous breast models. Phys. Med. 51, 99–107.
Sarno, A., Tucciariello, R.M., Mettivier, G., Di Franco, F., Russo, P., 2019. Monte Carlo calculation of monoenergetic and polyenergetic DgN coefficients for mean glandular dose estimates in mammography using a homogeneous breast model. Phys. Med. Biol. 64, 125012.
Sarno, A., Mettivier, G., di Franco, F., Paternò, G., Taibi, A., Cardarelli, P., et al., 2020. Advanced Monte Carlo application for in-silico clinical trials in x-ray breast imaging. In: 15th International Workshop on Breast Imaging (IWBI2020), vol. 11513. International Society for Optics and Photonics, 1151315.
Sarno, A., Tucciariello, R.M., Mettivier, G., Del Sarto, D., Fantacci, M.E., Russo, P., 2021a. Normalized glandular dose coefficients for digital breast tomosynthesis systems with a homogeneous breast model. Phys. Med. Biol. 66, 065024.
Sarno, A., Mettivier, G., di Franco, F., Varallo, A., Bliznakova, K., Hernandez, A.M., et al., 2021b. Dataset of patient-derived digital breast phantoms for in silico studies in breast computed tomography, digital breast tomosynthesis, and digital mammography. Med. Phys. 48, 2682–2693.
Sarno, A., Mettivier, G., Bliznakova, K., Hernandez, A.M., Boone, J.M., Russo, P., 2022. Comparisons of glandular breast dose between digital mammography, tomosynthesis and breast CT based on anthropomorphic patient-derived breast phantoms. Phys. Med. 97, 50–58.
Savi, M., Villani, D., Andrade, M.A.B., Rodrigues Jr., O., Potiens, M.P.A., 2021. Study on attenuation of 3D printing commercial filaments on standard X-ray beams for dosimetry and tissue equivalence. Radiat. Phys. Chem. 182, 109365.
Schopphoven, S., Cavael, P., Bock, K., Fiebich, M., Mäder, U., 2019. Breast phantoms for 2D digital mammography with realistic anatomical structures and attenuation characteristics based on clinical images using 3D printing. Phys. Med. Biol. 64, 215005.
Sechopoulos, I., 2013a. A review of breast tomosynthesis. Part I. The image acquisition process. Med. Phys. 40, 014301.
Sechopoulos, I., 2013b. A review of breast tomosynthesis. Part II. Image reconstruction, processing and analysis, and advanced applications. Med. Phys. 40, 014302.
Sechopoulos, I., Bliznakova, K., Qin, X., Fei, B., Feng, S.S.J., 2012. Characterization of the homogeneous tissue mixture approximation in breast imaging dosimetry. Med. Phys. 39, 5050–5059.

Shaheen, E., De Keyzer, F., Bosmans, H., Dance, D.R., Young, K.C., Ongeval, C.V., 2014. The simulation of 3D mass models in 2D digital mammography and breast tomosynthesis. Med. Phys. 41, 081913.

Sharma, D., Graff, C.G., Badal, A., Zeng, R.P., Sawant, P., Sengupta, A., Dahal, E., Badano, A., 2019. Technical Note: in silico imaging tools from the VICTRE clinical trial. Med. Phys. 46, 3924–3928.

Shi, L., Vedantham, S., Karellas, A., O'Connell, A.M., 2013. Technical note: skin thickness measurements using high-resolution flat-panel cone-beam dedicated breast CT. Med. Phys. 40, 031913.

Sikaria, D., Musinsky, S., Sturgeon, G.M., Solomon, J., Diao, A., Gehm, M.E., et al., 2016. Second generation anthropomorphic physical phantom for mammography and DBT: Incorporating voxelized 3D printing and inkjet printing of iodinated lesion inserts. In: Medical Imaging 2016: Physics of Medical Imaging, vol. 9783. SPIE, pp. 1581–1590.

Strudley, C.J., Young, K.C., Looney, P., Gilbert, F.J., 2015. Development and experience of quality control methods for digital breast tomosynthesis systems. Br. J. Radiol. 88, 20150324.

Sturgeon, G.M., Park, S., Segars, W.P., Lo, J.Y., 2017. Synthetic breast phantoms from patient based eigenbreasts. Med. Phys. 44, 6270–6279.

Thulasi, P.V., Joseph, A., Varier, K.M., 2021. Studies on partial and total photon interaction parameters in the energy range 1 keV–100 GeV of some synthetic polymers having medical applications. Radiat. Phys. Chem. 180, 109252.

Tomal, A., Costa, P.R., 2017. Phantoms for image quality and dose assessment. In: Handbook of X-Ray Imaging: Physics and Technology, vol. 4. CRC Press, London chap. 56, P. Russo.

Tucciariello, R.M., Barca, P., Del Sarto, D., Lamastra, R., Mettivier, G., Retico, A., et al., 2021. Voxelized breast phantoms for dosimetry in mammography. In: In Proceedings of the 14th International Joint Conference on Biomedical Engineering Systems and Technologies (BIOSTEC 2021) - Volume 3: BIOINFORMATICS, pp. 154–161.

Vancoillie, L., Cockmartin, L., Marshall, N., Bosmans, H., 2021. The impact on lesion detection via a multi-vendor study: a phantom-based comparison of digital mammography, digital breast tomosynthesis, and synthetic mammography. Med. Phys. 48, 6270–6292.

Varallo, A., Sarno, A., Castriconi, R., Mazzilli, A., Loria, A., Del Vecchio, A., et al., 2022. Fabrication of 3D printed patient-derived anthropomorphic breast phantoms for mammography and digital breast tomosynthesis: imaging assessment with clinical X-ray spectra. Phys. Med. 98, 88–97.

Villani, D., Rodrigues Jr., O., Campos, L.L., 2020. Dosimetric characterization of 3D printed phantoms at different infill percentages for diagnostic X-ray energy range. Radiat. Phys. Chem. 172, 108728.

Vimieiro, R.B., Borges, L.R., Caron, R.F., Barufaldi, B., Bakic, P.R., Maidment, A.D.A., Vieira, M.A.C., 2019. Noise measurements from reconstructed digital breast tomosynthesis. In: Conference on Medical Imaging - Physics of Medical Imaging. Feb 17-20, San Diego, CA.

Vollmar, S.V., Langner, O., Weigel, M., Bosmans, H., Kalender, W.A., 2009. Breast phantom design for dedicated breast CT and breast tomosynthesis. In: World Congress on Medical Physics and Biomedical Engineering. Springer, Berlin, Heidelberg, pp. 53–56. September 7-12, 2009, Munich, Germany.

White, D.R., 1978. Tissue substitutes in experimental radiation physics. Med. Phys. 5, 467–479.

White, D.R., Martin, R.J., Darlison, R., 1977. Epoxy resin based tissue substitutes. Br. J. Radiol. 50, 814–821.

Zhao, C., Solomon, J., Sturgeon, G.M., Gehm, M.E., Catenacci, M., Wiley, B.J., et al., 2017. Third generation anthropomorphic physical phantom for mammography and DBT: Incorporating voxelized 3D printing and uniform chest wall QC region. March. In: Medical Imaging 2017: Physics of Medical Imaging, vol. 10132. SPIE, pp. 479–486.

Zyganitidis, C., Bliznakova, K., Pallikarakis, N., 2007. A novel simulation algorithm for soft tissue compression. Med. Biol. Eng. Comput. 45, 661–669.